ELASTIC SCATTERING OF PROTONS FROM ^{64}Zn, ^{66}Zn, and ^{68}Zn BETWEEN 10 and 60 MeV

by

Shu-po Kwan

A thesis submitted to the Faculty of Graduate Studies of the University of Manitoba in partial fulfillment of the requirements for the degree of Master of Science.

June 1974

ELASTIC SCATTERING OF PROTONS FROM ^{64}Zn, ^{66}Zn, and ^{68}Zn BETWEEN 10 and 60 MeV

by

Shu-po Kwan

A dissertation submitted to the Faculty of Graduate Studies of the University of Manitoba in partial fulfillment of the requirements of the degree of

MASTER OF SCIENCE

ABSTRACT

An experiment was performed using the proton beam from the University of Manitoba sector focused cyclotron to study the scattering of protons by ^{64}Zn, ^{66}Zn, and ^{68}Zn. Elastic scattering differential cross sections were obtained with incident proton energies of 22.2MeV, 30.0MeV, and 39.6MeV. These data plus differential cross sections and polarization data that were available in the liturature for proton energies between 10 to 60 MeV were analysed with a standard optical model. Special interest was placed in the energy dependence and isospin dependence of the real central potential. The energy dependences for the three zinc isotopes were found to be almost the same. The values of the energy derivatives of the volume integral per nucleon ($\frac{dJ/A}{dE}$) obtained were around -4.53 and they were more negative than the A dependent trend set by previous ^{16}O, ^{40}Ca, and ^{208}Pb results. The isospin-dependent component of the real central potential was found to be much smaller (-3.8±2.5MeV) than the value usually accepted (24MeV). This suggested that nuclear structure effect may be important among the zinc isotopes.

ACKNOWLEDGEMENT

I would like to thank my supervisor Dr. N. E. Davison for his constant encourgement and advice throughout this work. I would also like to express my gratitude to Dr. J. Horton, Ms. H. Huang, and Mr. A. McDonald for their help in setting up the experiment and collecting the data.

CONTENTS

LIST OF FIGURES

LIST OF TABLES

CHAPTER ONE

INTRODUCTION

The real potential of the optical model has been found to be both energy and isospin dependent. The present thesis describes an experiment designed to study the optical model for elastic scattering of protons by zinc isotopes, with special interest placed in the energy and isospin dependence.

Chapter two gives a general description of the optical model potential. In particular some theoretical aspects of the nonlocality and isospin are discussed and some results obtained in these two areas in the past ten years are presented.

An experiment was performed using the proton beam from the University of Manitoba sector focused cyclotron. Enriched ^{64}Zn, ^{66}Zn, and ^{68}Zn targets were bombarded by protons at 22.2MeV, 30.0MeV, and 39.6MeV, and differential cross sections were measured. The experimental arrangement and data reduction are described in

chapter three.

The last chapter is divided into four sections. The first section discusses the differential cross sections obtained in this experiment. Section two gives the optical model analysis performed. Discussion of the energy dependence and isospin dependence is given in the third section and the last section gives a summary of the present study.

CHAPTER TWO

2.1 OPTICAL MODEL

In the study of nucleon-nucleus interactions, the complexity in solving the many-body problem does not allow one to deal with the process in detail, beginning from only the nucleon-nucleon interaction. In order to reduce the many-body problem to a two-body problem, various interactions are replaced by a potential acting between the incident particle and the target nucleus. In mathematical form the interaction would be described by Schrödinger's Equation as the following:

$$-\frac{\hbar^2}{2\mu}\nabla^2\psi + U(r)\psi = E\psi \qquad (1)$$

where $U(r)$ is the potential, E and μ are the centre of mass energy and the reduced mass of the incident particle respectively.

In order to take into account inelastic scattering and other possible reactions $U(r)$ has

to be in complex form. Absorption in all inelastic processes permitted by the Pauli Principle and by the law of conservation of energy is described by the imaginary part.

About twenty years ago, the square well potential was used for its simplicity(Fe54) but it was found to predict too small a reaction cross section and to give too much scattering at the backward angles. This indicates that the potential should not have a sharp cut off but should instead go to zero gradually. The form proposed by Woods and Saxon (Wo54) has been generally used. The potential is expressed as

$$U(r) = - (V_o + iW_o) \left[1 + \exp(\frac{r-R}{a})\right]^{-1} \qquad (2)$$

where R and a are called the nuclear radius and diffuseness.

Equation (2) gives only a very simple expression for the potential. In order to account for polarization effects and the coulomb interaction, more terms were added to form the so-called standard optical model (SOM) potential which is composed of

(1) the real central potential

$$- V f (r, r_o, a_o)$$

(2) the central imaginary potential

surface part $\quad i4a_I W_D \left(-\frac{d f(r, r_I, a_I)}{dr}\right)$

volume part $\quad -iWf(r, r_I, a_I)$

(3) the spin-orbit potential

$$(V_{so}+iW_{so}) \left(\frac{\hbar}{m_\pi c}\right)^2 \frac{1}{r} \frac{d f(r, r_{so}, a_{so})}{dr} \bar{L}\cdot\bar{\sigma}$$

(4) the coulomb potential

$$\frac{Zze^2}{2R_c}\left[3 - \left(\frac{r}{R_c}\right)^2\right] \qquad \text{for } r \leqslant R_c$$

$$\frac{Zze^2}{r} \qquad \text{for } r \geqslant R_c$$

The function $f(r,r',a')$ is the Woods-Saxon form factor given by

$$f(r,r',a') = \left[1 + \exp \frac{r - r'A^{1/3}}{a'}\right]^{-1}$$

The symbol $\bar{L}$ is the orbital angular momentum of the l^{th} partial wave and $\bar{\sigma}$ is two times the spin of the incident particle; m_π is the mass of π meson and Z and z are the charges of the target and the incident particle respectively.

The addition of the surface imaginary term to the potential was based on the following argument: Absorption is the result of nucleons in the nucleus being excited to higher energy levels. As most of the states in the interior of the nucleus are filled, excitation of the nucleons there is unlikely unless the incident energy is

high enough that the nucleons would be excited to much higher energy levels. Therefore, at low bombarding energies, one would expect the absorption to take place in preference at the surface of the nucleus. The derivative Woods-Saxon form is usually used to represent this surface imaginary term and it is customarily taken to have the same geometrical parameters r_I and a_I as the volume imaginary part.

The spin-orbit potential was added to account for the polarization of the scattered nucleons. This spin-orbit potential also improved the fits to the differential cross sections by damping out unphysically large oscillations arising at large angles when only the central potential was used. The multiple scattering approximation used by Kerman et al (Ke59) indicated that the spin-orbit potential should also be complex, with the imaginary part having a maximum strength of about one-third of the real part. From phenomenological analysis, however, the imaginary spin-orbit potential does not seem to be necessary except at high energy.

The coulomb potential is obtained by considering the nucleus as a uniformly charged sphere with radius R_c.

All 11 parameters (five dynamical parameters V, W, W_D, V_{so}, W_{so}, and six geometrical parameters r_o, a_o, r_r, a_r, r_{so}, a_{so}) in expression (3) can be obtained from a least square fit to the experimental data —— minimization of χ^2 which is given by

$$\chi^2 = \sum^{N}\left(\frac{\sigma_T(\theta)-\sigma_E(\theta)}{\delta\sigma_E(\theta)}\right)^2$$

Here the theoretical differential cross sections are $\sigma_T(\theta)$ and the experimental data are $\sigma_E(\theta)\pm\delta\sigma_E(\theta)$. When polarization data are available, they may also be included in the calculation of χ^2.

Unfortunately, this analysis does not give a unique set of parameters for each set of experimental data. It is found that there are functions of some of the parameters such that χ^2 is very insensitive to variations in the parameters provided the functions remain constant. The most important of these relationships is called the Vr_o^n ambiguity. When the kinetic energy of the incident particle is below about 100MeV, one can vary V and r_o without changing χ^2 appreciably provided Vr_o^n=constant (n is between 2 and 3). This is true as long as r_o is restricted to

$1.0 \leqslant r_o \leqslant 1.4$ (Ho67). The imaginary potential W_D and the diffuseness a_I make up another pair of parameters which causes an ambiguity similar to that of Vr_o^n . Ambiguities such as the two mentioned are connected with nuclear structure (Ho66). The product $W_D a_I$ is correlated with the nuclear deformation (He70). Therefore, when obtaining potential strength parameters for different sets of experimental data in order to intercompare them, the geometric parameters are usually kept fixed.

2.2 NONLOCALITY AND ISOSPIN DEPENDENT

From the theoretical derivation done by Feshbach (Fe58) one could notice that the optical model is nonlocal. The Schrodinger equation should therefore take on the integrodifferential form

$$\frac{\hbar^2}{2\mu}\nabla^2\psi(\bar{r}) + E\psi(\bar{r}) - \int V(\bar{r},\bar{r}')\psi(\bar{r}')d\bar{r}' = 0$$

where $V(\bar{r},\bar{r}')$ is the nonlocal potential. As $V(\bar{r},\bar{r}')$ must be symmetric in $\bar{r}$ and $\bar{r}'$ and the range β of the nonlocality is small, Perey and

Buck chose

$$V(\bar{r},\bar{r}') = V\left(\frac{1}{2}|\bar{r}+\bar{r}'|\right)\frac{1}{(\pi\beta^2)^{3/2}}\exp\left[-\left(\frac{\bar{r}-\bar{r}'}{\beta}\right)^2\right]$$

to facilitate numerical calculation (Pe62). This non-local potential was used by Perey and Buck to analyse neutron scattering data up to 25MeV and by Schulz and Wiebicke (Sc66) to study proton elastic scattering. Both of them found good overall fits. On the other hand, Perey and Buck showed that one can use a local potential to fit differential cross sections quite accurately. They also showed that the relation between the equivalent local potential $V_L(r)$ and non-local potential $V_N(r)$ is approximately

$$V_N(r) = V_L(r)\exp\left[+\frac{\mu\beta^2}{2\hbar^2}\left(E-V_L(r)\right)\right]$$

By first order expansion in E, one obtains

$$V_N(r) = V_L(r)\left[1 + \frac{\mu\beta^2}{2\hbar^2}\left(E-V_L(r)\right)\right]$$

This explains in part the energy dependence of the potential strength of the optical model when the local potential is used (Theoretical derivation of

the optical model performed by Fesbach showed that the optical model is intrinsically energy dependent apart from nonlocality).

In 1962, Lane (La62) showed that the nuclear potential should have an isospin dependent term given by $A^{-1}(\bar{t}.\bar{T})V_1$. The factor $(\bar{t}.\bar{T})$ comes from averaging over the constituent two-body Heisenberg exchange forces. The total isospin of the nucleon-nucleus system can have the values $T+\frac{1}{2}$ and $T-\frac{1}{2}$, and the corresponding eigenvalues of $(\bar{t}.\bar{T})$ are $\frac{1}{2}T$ and $-\frac{1}{2}(T+1)$ respectively. Both these isospin states are possible for proton scattering. Therefore the nuclear potential is obtained by averaging them with weight factors $(2T+1)^{-1}$ and $2T(2T+1)^{-1}$ the average isospin potential is thus found to have the form

$$-\frac{1}{2}\frac{V_1 T}{A} .$$

As nuclei are predominantly in the state of minimum isospin with $T=T_z=\frac{1}{2}(N-Z)$, the isospin dependent term for proton scattering is taken to be

$$-\frac{1}{4}\frac{N-Z}{A}V_1$$

assuming the proton and neutron distributions have the same shape. For neutron scattering, only the

$T+\frac{1}{2}$ state is allowed and the corresponding isospin potential is

$$+ \frac{1}{4} \frac{N-Z}{A} V_t$$

As the isospin interaction can cause charge-exchange reactions (depolarization of isospin) the form and magnitude of the isospin potential can be determined by analysing the cross section of (p,n) reactions to the isobaric analogue states of the target nucleus. From such analysis, it is found that the isospin term is more likely to have a surface form than a volume form and that V_t is approximately 30MeV. Unfortunately there are not enough (p,n) data for a comprehensive study of the isospin potential. As $\frac{N-Z}{A}$ is generally < 0.2 the isospin term is quite small and does not have any 1st order effect on the differential cross section. It is usually taken to have the same volume form as the real central potential and is analysed as a component of the real central potential. This approximation tends to increase the radius of the volume form but its effect is quite hard to notice due to the Vr_o^n ambiguity.

In 1970 Sinha and Edwards (Si70) fitted

elastic scattering data with a real surface term and substantial fit improvement was claimed. This derivative real model (DRM) has been adopted by some authors but their results have not yet been able to give more information concerning the isospin term in the optical model potential. Boyd et al(Bo72) found that there was an appreciable derivative term even in N=Z nuclei. It was suggested that, other than the isospin, the real derivative term is also attributable in part to the exchange, target polarization and the hard core of the effective nucleon-nucleon interaction, which are all difficult to calculate. On top of this, the idea of using the real derivative term to study the isospin dependence was futher discouraged by the study of Zimanji and Gyrmali (Zi68). By folding the excess neutron distribution of the shell model with an effective two-body isospin dependent force, they found that the symmetry potential appeared to have a pure derivative Woods-Saxon shape only for nuclei with a small neutron excess. As it is not surprising to obtain improved fits after adding 3 more parameters, there is some scepticism about the validity of the addition term used in (Si70) and (Bo72).

More than a decade ago, attempts were made to determine overall proton potentials. In 1963, Perey analysed elastic scattering data for 9-22 MeV protons incident on a wide range of nuclei. The following generalized parameters were obtained:

$$V = 53.3 - 0.55E + 27\frac{N-Z}{A} + 0.4\frac{Z}{A^{1/3}} \quad \text{(MeV)}$$

$$W_D = 3A^{1/3};\ W = 0.0 \quad \text{(MeV)}$$

$$V_{so} = 8.5\,(E \geq 17\text{MeV});\ V_{so} = 7.5\,(E < 17\text{MeV}) \quad \text{(MeV)}$$

$$r_o = 1.25;\ r_I = 1.25;\ r_{so} = 1.25 \quad \text{(fm)}$$

$$a_o = 0.65;\ a_I = 0.47;\ a_{so} = 0.65 \quad \text{(fm)} \qquad (6)$$

The energy dependence was taken to be linear (-0.55E). However, Perey showed that -0.55 is actually too small due to the effect of coupling the elastic channel to the first inelastic channel and the value without coupling would be -0.3. The last term of V in (6) is the coulomb dependence which arises from the energy dependence of the nuclear potential in the presence of the coulomb field. The coefficient 27MeV for the symmetry term was obtained from the linear fit of $V-0.4Z/A^{1/3}$ vs $\frac{N-Z}{A}$.

A more recent and complete work along these lines was done by Becchetti and Greenlees (Be69). After analysing a large number of nucleon elastic scattering data for nuclei with mass $A > 40$

and bombarding energy E< 50MeV in a simultaneous search, they obtained the following parameters for the proton standard optical Model:

$$V = 54.0 - 0.32E + 0.4\frac{Z}{A^{1/3}} + 24.0\frac{N-Z}{A} \quad \text{(MeV)}$$

$$W = 0.22E - 2.7 \quad \text{(MeV)}$$

(or zero which ever is greater)

$$W_D = 11.8 - 0.25E + 12.0\frac{N-Z}{A} \quad \text{(MeV)}$$

(or zero which ever is greater)

$$V_{so} = 6.2 \quad \text{(MeV)}$$

$$r_o = 1.17; \quad a_o = 0.75 \quad \text{(fm)}$$

$$r_I = 1.32; \quad a_I = 0.51 + 0.7\frac{N-Z}{A} \quad \text{(fm)}$$

$$r_{so} = 1.01; \quad a_{so} = 0.75 \quad \text{(fm)}, \quad (7)$$

One can notice that the imaginary potential is taken to be isospin dependent as well.

In 1968, the analysis of elastic scattering of 11MeV protons from 24nuclei in the range ^{45}Sc to ^{76}Ge (Pe68)cast doubt on the validity of parametrizing the real potential in terms of the isospin in that energy and mass range. When the real central potential is plotted against $\frac{N-Z}{A}$, the data points seem to fall on a family of hyperbolic curves, one for each isospin. Morever, the real potentials show a linear dependence on A. The reformulated optical model (ROM) proposed by Greenlees et al (Gr68) provides some explanation to Perey's result. The volume

integral of the real potential which is given by

$$J = \frac{4\pi R^3 V}{3}\left(1 + \frac{\pi^2 a^2}{R^2}\right) = jA$$

for the Woods-Saxon potential form was found to be proportional to A. One could express the real potential in the form

$$V = \frac{3jA}{4\pi R^3\left(1+\frac{\pi^2 a^2}{R^2}\right)} = \frac{3j}{4\pi r_o^3\left[1+\frac{\pi^2 a^2}{r_o^2}\left(\frac{\alpha}{2T}\right)^{2/3}\right]}.$$

In the latter expression R is replaced by $r_o A^{1/3}$ and A by $\frac{2T}{\alpha}$ with $T = \frac{1}{2}(N-Z)$ and $\alpha = \frac{N-Z}{A}$. This gives a family of curves each characterized by a different value of T as observed by Perey. These results might suggest that the isospin term that is being studied can be interpreted as the A dependence when the geometrical parameters are assumed to be fixed. However this cannot be the only source of isospin dependence as it gives no account of the isospin potential necessary to describe the (p,n) reactions.

Hodgson (Ho70) considered this problem to be the result of restricting the nuclear radius to be proportional to $A^{1/3}$. He wrote the real potential in the form

$$V = \frac{kA}{R^3\left(1+\frac{\pi^2 a^2}{R^2}\right)} + 24\alpha + \frac{0.517T(1-\alpha)}{\alpha R} \qquad (8)$$

The first term in (8) is based on the A dependence of the volume integral. The coefficient of the second term, i.e. the isospin dependent term, is obtained from (p,n) reactions and the last term corresponds to the coulomb dependent term $0.4Z/A^{1/3}$. Using this formula Hodgson searched for an expression for R which would fit Perey's real potential. He obtained

$$R = 1.204A^{1/3} + 0.305$$

but when he included data from other analyses he had to express the radius in the form

$$R = -0.11A + 1.61A^{2/3} - 6.30A^{1/3} + 11.59$$

This formula is hard to interpret physically.

The energy dependent terms in the real central potentials obtained by Perey and Becchetti were the results of analysing elastic scattering data with a wide range of nuclei. Work has also been carried out to determine the energy dependence for individual nuclei and as shown in Table I , it seems to be different for different isotopes. This casts doubt on the validity of finding the energy dependence and isospin dependence simultaneously.

In previous studies of the isospin dependence, the details of nuclear structure were

not taken into consideration. It was assumed that nuclear structure effects would be smoothed out when a wide range of nuclei was used.

The isospin dependence has also been studied for isotopic sequences. One advantage of using isotopic sequences is that the coulomb correction term is almost the same for all the nuclei studied (Be64). On the other hand, the nuclear structure effects would strongly affect the isospin term and the isospin dependence obtained this way seems to have a wider fluctuation.

Some of the studies with isotopic sequences have shed some light on the nuclear structure effects. When studying the tin isotopes at 9.8MeV(Du65) and at 16MeV(Ma68) the real potential was found to increase up to ^{114}Sn and fall at ^{116}Sn, and then increase again with mass number. Sood(So65) suggested that this may be explained by the change of shell occupied by the outermost nucleons at ^{116}Sn. This explanation could also be applied to the Zirconium isotopes studies by Mani et al (Ma71). The study of Samarium isotopes (Fu70) revealed another dependence of the real potential. The real potential increases from ^{144}Sm to ^{148}Sm but it

dropped and remained quite constant for ^{150}Sm, ^{152}Sm, and ^{154}Sm. Fulmer et al considered this unusual result as resulting from the deformation of the isotopes.

2.3 OBJECTIVE OF THE PRESENT EXPERIMENT

As the zinc isotopes have no change in shells nor drastic change in deformation (see Table Ia), one may expect a priori that the study of isospin dependence would not be affected by nuclear structure effects. Angular distributions were obtained for proton elastic scattering at incident energies of 22.2MeV, 30.0MeV, and 39.6MeV for ^{64}Zn, ^{66}Zn, and ^{68}Zn. When combined with data obtained from the literature for proton energies of 11.0MeV(Pe68), 14.5MeV(Ke64), and 49.08MeV(Ca67) for all three isotopes and 61.4MeV(Fu69) for ^{68}Zn, data covering the range from 10MeV to 50MeV in 10MeV steps were available. The energy dependence of these three zinc isotopes was first obtained. This provides two kinds of information that we are interested in: 1)whether the energy dependence of the zinc isotopes follows the A dependent trend as indicated in Table I and, 2)how much the energy dependence changes from one

zinc isotope to another.

The isospin dependence was then studied. As there are only three data points for each energy, the isospin dependence determined at each energy was of limited accuracy. A more accurate approach is to find the energy dependence and isospin dependence simultaneously. This approach would be justified if the energy dependences for the three zinc isotopes were found to be almost the same.

TABLE I

	Energy range (MeV)	dV/dE	ref.
^{6}Li	25 - 50	-0.35	Lo70
^{16}O	20 - 55	-0.37±0.04	Va69
^{40}Ca	20 - 180	-0.28±0.03	Va71
^{208}Pb	16 - 180	-0.31±0.03	Va74

TABLE Ia

The nuclear deformation factors of the zinc isotopes. (Ca67)

	β_2
^{64}Zn	0.24
^{66}Zn	0.23
^{68}Zn	0.21

β_2 is defined as in

$$R = R_0 (1 + \beta_2 Y_2^0 + \ldots\ldots)$$

CHAPTER THREE

3.1 EXPERIMENTAL ARRANGEMENT

The proton beam for the experiment was produced by the University of Manitoba sector focused cyclotron (Bu65). Figure 1 shows the layout of the beam facility used. The present experiment was performed on the 45°-left beam line.

After leaving the cycloton, the proton beam is deflected down the beam line by the combination magnet C. Along the beam line there are quadrupoles and steering magnets which guide the proton beam to the bending magnet. A set of slits (Slits 1) located at the waist produced by the first set of quadrupoles defines the object plane in front of the bending magnet. When passing through the bending magnet, the proton beam is momentum analyzed by a 45° deflection. A second slit system (Slits 2) at the focal plane of the magnet defines the suitable component of the beam that enters the experimental area where the quadrupole doublet Q7-Q8 produces a waist at the

Fig. 1 Cyclotron and beam line layout

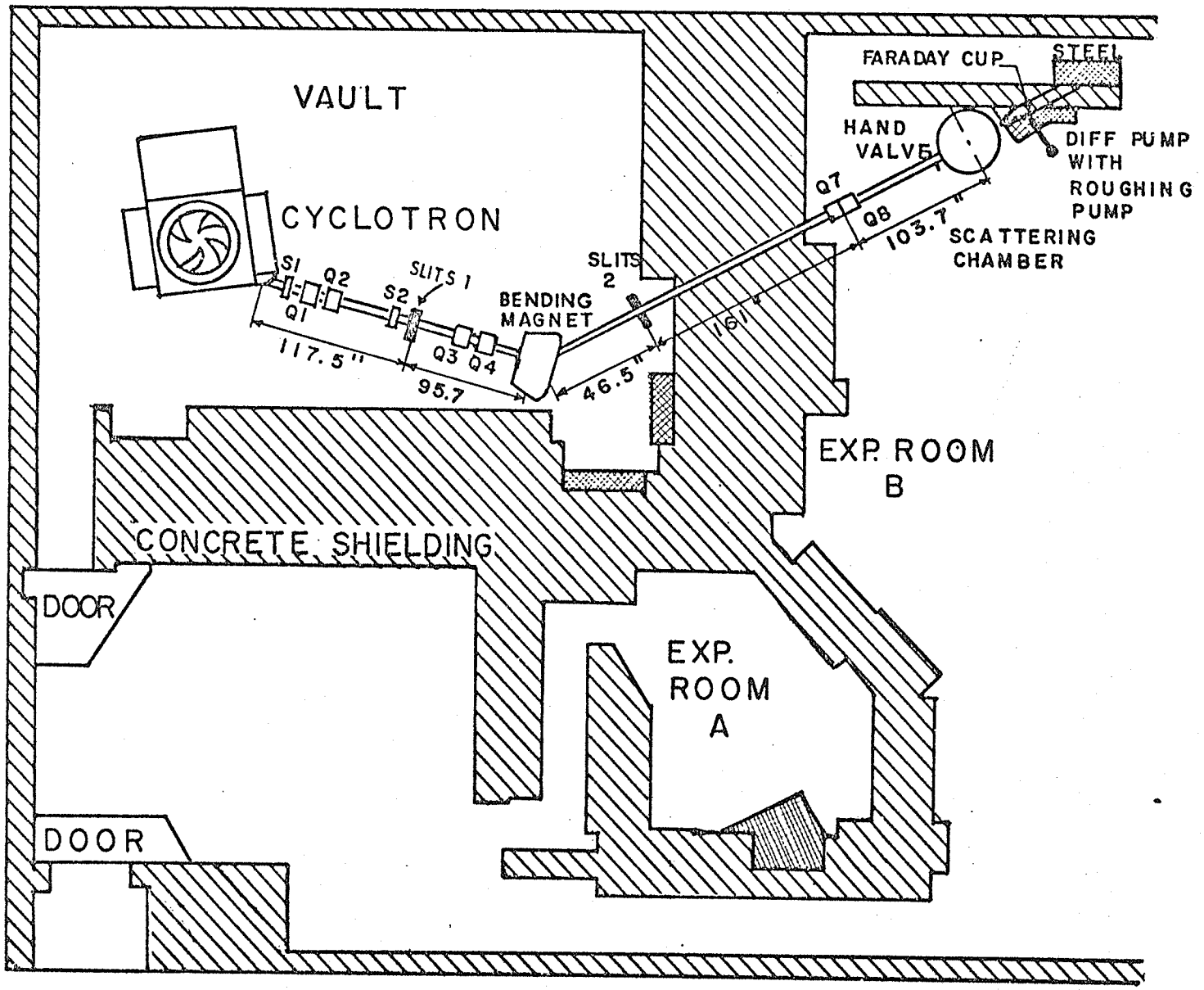

CYCLOTRON BEAM LINE LAYOUT

FIG. 1

centre of the 46-inch scattering chamber. In order to reduce the γ-ray background from the slit system, two lead collimators with 3.81 cm circular apertures and lengths of 5.08cm and 7.62cm respectively are placed inside the beam pipe immediately before the scattering chamber. Lead shielding also surrounds the beam pipe at the entrance to the scattering chamber.

A sketch of the scattering chamber is given in Fig. 2. The crescent shaped detector box is attached on a turn table which can be rotated from -180° to $+180^{\circ}$. Inside the detector box, eight NaI(Tl) scintillation counters are arranged to permit detection of scattered protons at eight angles simultaneously. Each detector consists of a NaI(Tl) scintillation crystal (3.81cm in diameter and 1.27cm thick) optically coupled to a photomultiplier tube (RCA4523) and is placed behind one of the eight windows on the inner arc of the detector box. All eight windows are covered by 0.0051cm Kapton-H foil. The detector box is maintained at atmospheric pressure when the scattering chamber is pumped down. In front of each window interchangeable collimators can be mounted. With the help of a theodolite, the detector box was carefully positioned such that

Fig. 2 Scattering Chamber. The detector box shown holds 8 detectors.

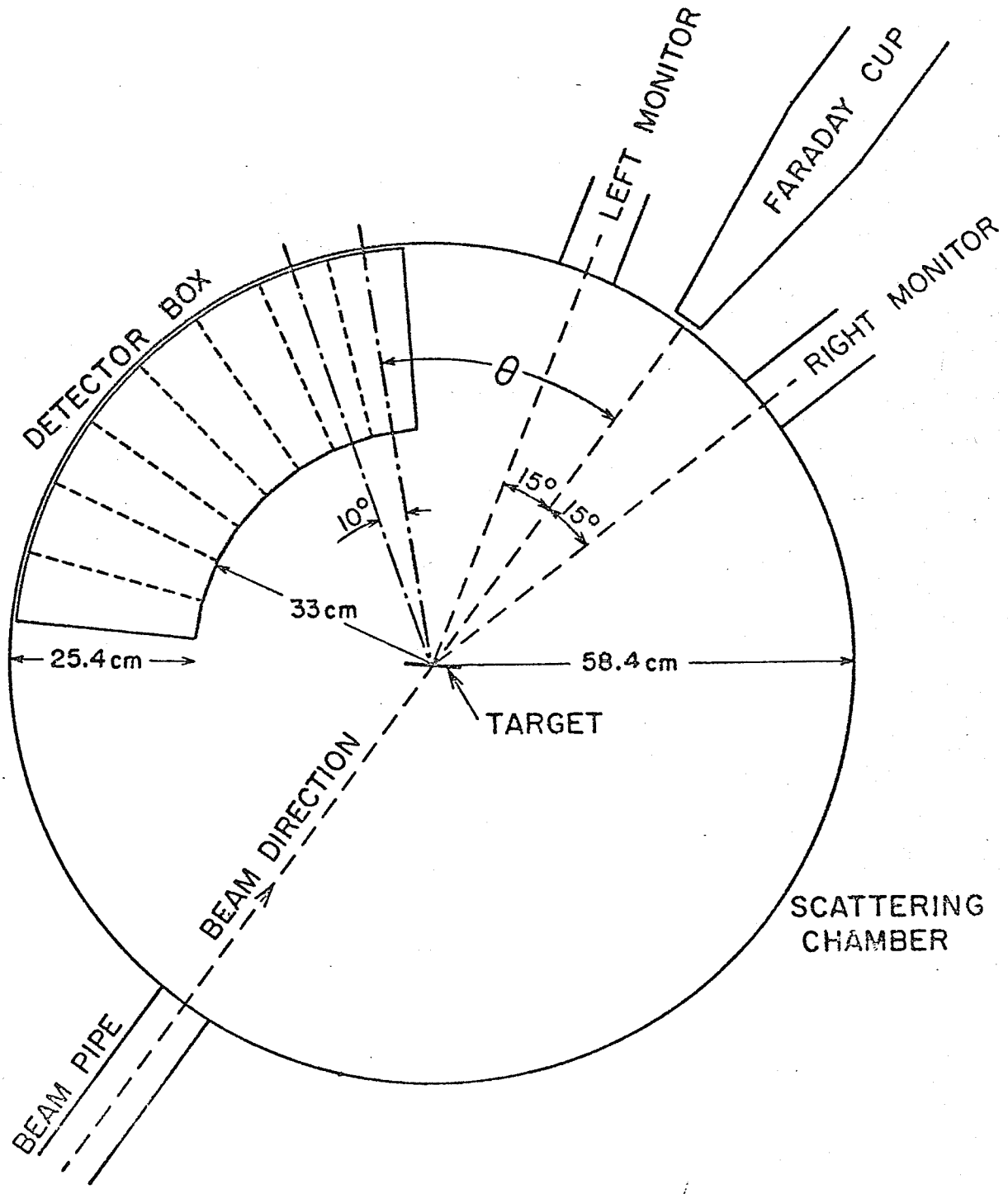

FIG. 2 SCATTERING CHAMBER

the apertures on the collimators were separated by 10.00° ±0.01° with respect to the centre of the chamber.

The turn table can be rotated either from the experimental room or remotely from the control room. An angular readout system gives the angular position of the first detector with an accuracy of ±0.01°.

At the top of the chamber there is a vacuum lock through which a target ladder can be lowered into the chamber. The target ladder used can hold five targets.

A plastic scintillator was mounted on this target ladder so that when it was placed in the path of the beam the position and size of the beam spot at the centre of the chamber could be examined via closed-circuit television. The actual beam spot shape and size were obtained from glass slide exposures made at the target position and at the beam entrance to and exit from the scattering chamber. It was found to be almost rectangular in shape and typically about 0.25cm wide by 0.60cm high at the target position. The beam divergence was typically ±0.8° about the beam axis in the horizonal direction and there was no divergence in the vertical plane.

To ensure that the beam travelled along the 0° line of the scattering chamber, two NaI(Tl) scintillation counters were set at 15° to the left and to the right of the beam direction. The beam spot was adjusted such that the difference between the number of counts detected by the two 15° monitors was less than 3%. Additional checks were made by comparing elastic yield obtained when the detector box was placed on the left and right hand sides of the scattering chamber.

After passing through the scattering chamber, the proton beam was collected by the Faraday cup. The Faraday cup was connected to a current indicator and charge integrator (Brookhaven Instrument Corp. model 1000). The digital signals from the charge integrator were recorded by a fast scaler.

As only four analog to digital converters (ADC) were used for eight detectors, signals from two detectors were mixed together and fed into one ADC. The signals were routed within the on-line computer used for data collection by a signal generated as described below. The typical electronic set up for a pair of detectors is shown in Fig. 3. The amplifiers have two outputs each.

Fig. 3 The electronic set up for a pair of detectors.

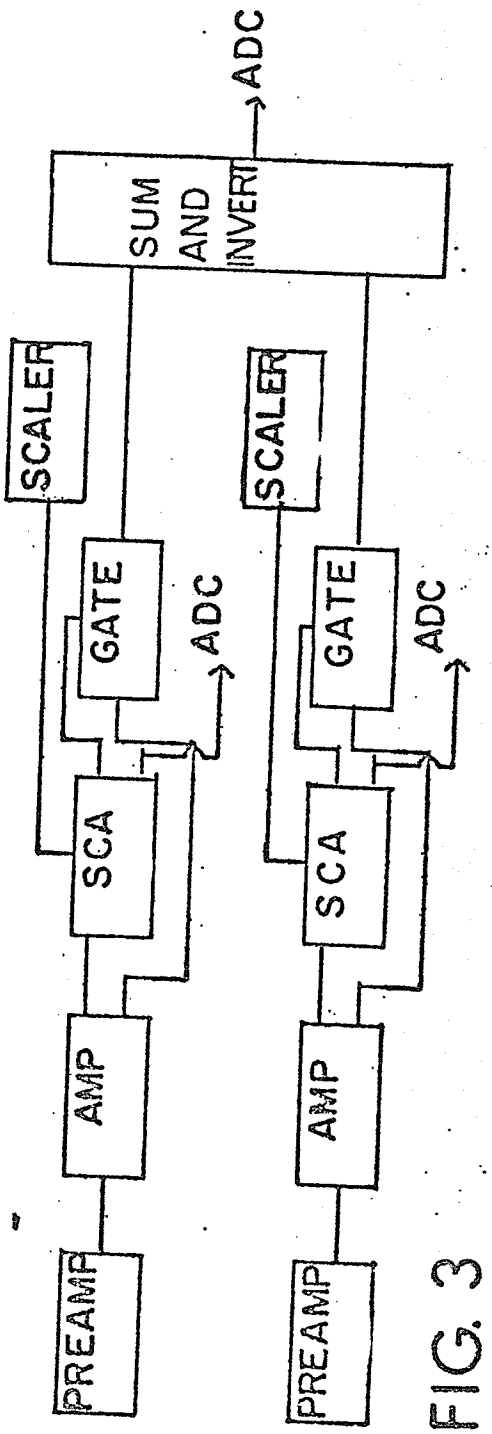
ADC
SUM AND INVERT
SCALER
SCALER
GATE
GATE
ADC
ADC
SCA
SCA
AMP
AMP
PREAMP
PREAMP

FIG. 3

The prompt bipolar outputs were fed into the timing single channel analysers (TSCA) and the delayed unipolar outputs were sent to the linear gates. Outputs from the TSCA's had three functions. Firstly, they opened the linear gates so that the desirable linear pulses could pass through. Secondly, they were use to route signals sent to the ADC. Thirdly, they were sent to fast scalers. The outputs of two linear gates were mixed in a sum and invert amplifier and then fed into an ADC. The ADC's were interfaced to a PDP15/40 computer where the spectra from the eight detectors were stored in eight memory regions of 512 channels each. The counts in the fast scalers were used to give the correction factor for the dead time of the ADC's. The dead time correction factor was taken to be the ratio of the counts recorded by the scaler to the total number of counts in the corresponding spectrum recorded by the computer. A typical spectrum is shown in Fig. 4.

The targets used were self supporting foils with the following characteristics.

	Measured Thickness	purity
^{64}Zn	4.794±0.019 mg/cm^2	99.66%
^{66}Zn	4.681±0.028 mg/cm^2	98.55%
^{68}Zn	4.996±0.040 mg/cm^2	98.50%

Fig. 4 The spectrum of $p+^{64}Zn$ at $\theta_{lab} = 75.0^{\circ}$ with E = 22.2MeV.

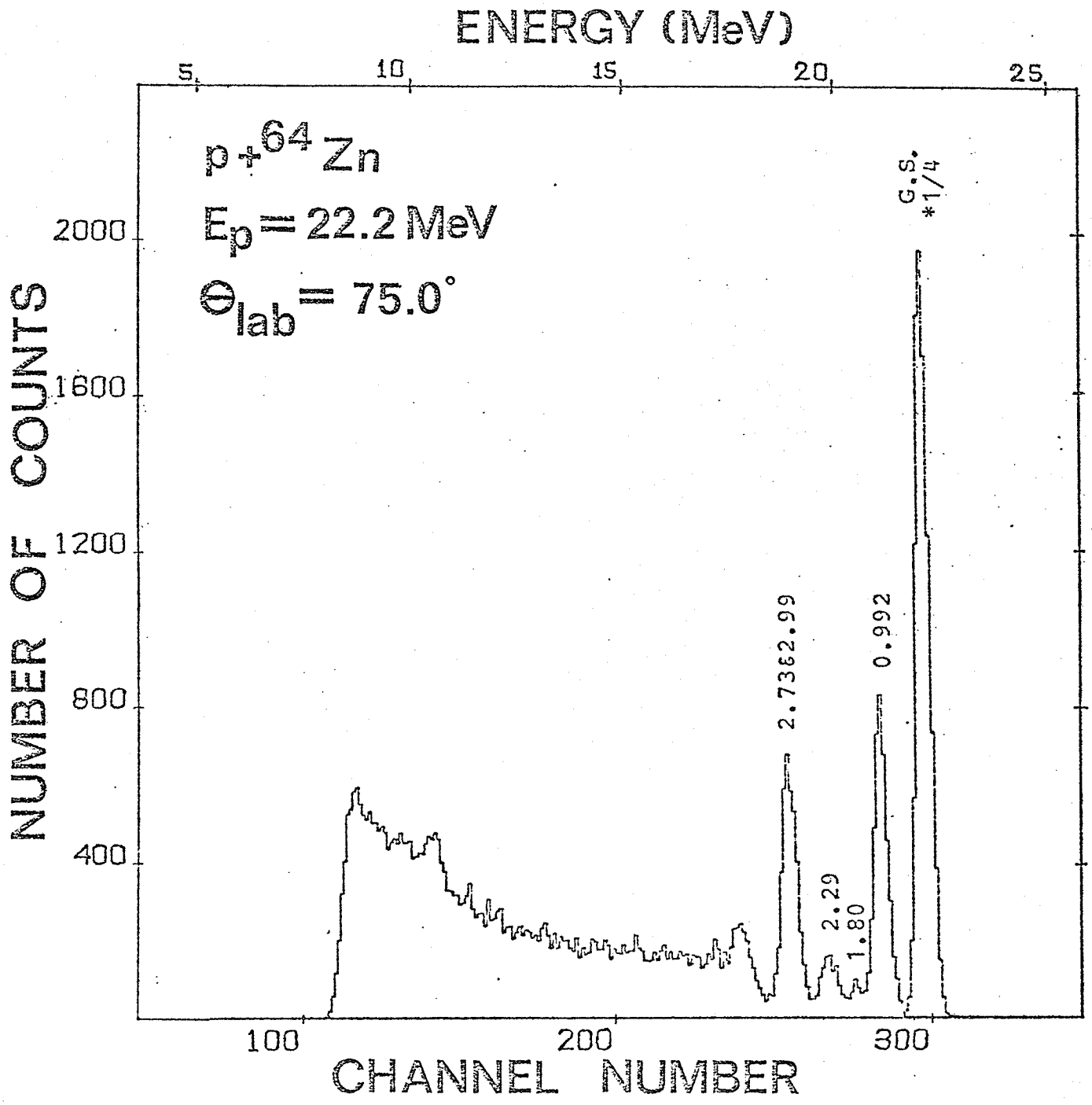
ENERGY (MeV)
5
10
15
20
25
p + 64 Zn
Ep = 22.2 MeV
Θlab = 75.0°
G.S.
*1/4
0.992
2.73±2.99
2.29
1.80
NUMBER OF COUNTS
2000
1600
1200
800
400
100
200
300
CHANNEL NUMBER

Fig. 4

The weight of the target was measured using a micro-balance and accuracy within 0.005% was obtained. The length and width of the rectangular targets were obtained by taking measurement along the edges using a vernier caliper. The error in these measurements was about 0.3%.

The energy of the proton beam was related to the bending magnet field strength, which was determined by using an NMR system. The energy calibration of the bending magnet was determined using the cross-over method with CD_2 and CH_2 targets (Sm64). The uncertainty of the beam energy was about ±150keV.

3.2 DATA REDUCTION AND ERRORS

The differential cross section for the scattering of a beam of incident particles by a single scattering center is defined by

$$\frac{d\sigma}{d\Omega} = \frac{\eta(\theta)}{I_o}$$

where $\eta(\theta)$ is the number of particles scattered per unit time into the unit solid angle about θ and I_o is the incident flux. Taking Y to be the number of protons scattered into the solid angle $\Delta\Omega$

during the time ΔT by n_t target atoms, then

$$\eta(\theta) = \frac{Y}{n_t \, \Delta\Omega \, \Delta T} .$$

The incident proton flux is given by

$$I_o = \frac{Q}{eS\Delta T}$$

where e is the charge of the proton, S is the area of the target illuminated and Q is the charge collected in time ΔT. As the thickness t of the target can be express in the form

$$t = \frac{An_t}{NS} \qquad (\text{in mg/cm}^2)$$

where A is the atomic mass and N is Avogradro's number, the differential cross section can be expressed by

$$\frac{d\sigma}{d\Omega} = \frac{e}{N} \frac{AY}{Qt\Delta\Omega}$$

Putting in the values of e and N, the differential cross section becomes finally

$$\frac{d\sigma}{d\Omega} = 2.660 \times 10^{-4} \frac{AY}{Qt\Delta\Omega} \qquad \text{mb/sr}$$

In order to take into account the fact that the target is not usually perpendicular to the beam and the proton beam has finite size and divergence, $\Delta\Omega$ is replaced by a geometric factor G (Wi66) given by

$$G = G_o \left(1 + \Delta_o + \frac{\left(\frac{d\sigma}{d\Omega}\right)'}{\left(\frac{d\sigma}{d\Omega}\right)}\Delta_1 + \frac{\left(\frac{d\sigma}{d\Omega}\right)''}{\left(\frac{d\sigma}{d\Omega}\right)}\Delta_2 + \ldots\right).$$

Here $(\frac{d\sigma}{d\Omega})'$ and $(\frac{d\sigma}{d\Omega})''$ are the first and second derivatives of the differential cross section with respect to the scattering angle θ, and

$$G_o = \frac{\Delta\Omega}{\cos\phi} .$$

In G_o, ϕ is the angle between the normal to the target and the incident beam direction. The values of Δ_o, Δ_1, and Δ_2 may be obtained from the expressions given by Willmes (Wi66;Br71).

The relative errors in the differential cross section were calculated from the following:

1) Statistical error due to the counting statistics was obtained from $\frac{1}{\sqrt{Y}}$. Here, Y was the number of counts in the elastic peak with the background subtracted. Generally the statistical error was less than 1% in the forward angles and less

than 2% in the backward angles.

2) Error arising from the uncertainty in the scattering angles θ was calculated using

$$\Delta \left(\frac{d\sigma}{d\Omega} \right) = \left(\frac{d\sigma}{d\Omega} \right)' \Delta\theta$$

Here, $\Delta\theta$ was the uncertainty in θ. This error was usually around 1% in the forward angles and .2% in the backward angles except that there were one or two points at extreme forward angles which had errors of the order of 1.5%.

3) Error in the dead time correction was usually less than .4% except at the most forward angles where it might get as high as 1.5%. This error was calculated with the assumption that the uncertainty in the number of counts lost due to dead time was $\sqrt{\text{the number of counts lost}}$.

4) Error resulting from the uncertainty of energy (ΔE) was calculated from

$$\frac{d\left(\frac{do}{d\Omega}\right)}{dE} \Delta E$$

This error showed the largest variation of all the errors but it was generally less than 3%.

The total relative error for each data point was obtained by adding the above errors in quadrature,

and it was usually less than 2%. The absolute errors in the differential cross sections were determined from the following:

1) Error in measuring the solid angle was less than 0.9%.

2) Error in measuring the target thickness was given in section 3.1.

3) The uncertainty in setting the target angle gives rise to the error of target thickness seen by the proton beam. As this angular uncertainty is $\pm 0.5^{\circ}$, the corresponding error would be ±0.6% when the target is set at 60° or 120° with respect to the beam direction.

4) Error coming from the beam current integration was taken to be 1%.

The total absolute error was obtained by adding the above errors in quadrature.

CHAPTER FOUR

4.1 RESULTS

The elastic scattering differential cross sections for ^{64}Zn, ^{66}Zn, ^{68}Zn obtained in this experiment are tabulated in the appendix and their ratios to the Rutherford cross sections are shown in Fig. 8 to Fig. 10. When the error bars are not shown explicitly the experimental error bars would be smaller than the size of the dots.

It can be noticed that, as the proton energy increases, the diffraction-like structure becomes more pronounced and the minima in the angular distribution shift to smaller angles. This behaviour of the differential cross sections is also observed with the increase of neutron number at any particular energy. Futhermore, when differential cross sections for the three isotopes at 22.2MeV are compared, the differential cross sections for ^{68}Zn are found to be larger than those for ^{64}Zn at the forward angles but smaller at the backward angles. This phenomenon is completely reversed at 39.6MeV. This was

investigated further by comparing the 11MeV data (Pe68) and 49.08MeV data (Ca67) and they all suggest that there is a transition around 30MeV; when the incident energy is below this transition, differential cross sections increase at the forward angles but decrease at the backward angles with the increase in neutron number, and the reverse is true at higher energies.

In the literature there exist proton elastic scattering differential cross sections for ^{64}Zn, ^{66}Zn and ^{68}Zn at 39.6MeV obtained by Liers et al (Li70), and p+^{68}Zn data at 40MeV by Fricke (Fr67). They were plotted with the 39.6MeV data of this experiment for comparision (Fig.5 to Fig.7). The ^{64}Zn data of the present experiment show very good agreement with those of Liers et al. The absolute cross sections obtained in the present work for ^{66}Zn are slightly ($<$10%) smaller than those of Liers et al. Among the three sets of data for ^{68}Zn, the present data and those of Liers et al agree with each other but the data by Fricke et al are considerably lower (15%-20%). On the whole, all these data have almost the same shapes and phases of oscillations for each isotope; it is in only the absolute normalization that discrepancies occur. It should be pointed out,

Fig. 5 The differential scattering cross sections divided by the Rutherford cross section for the elastic scattering of protons from ^{64}Zn at 39.6MeV obtained in the present experiment are compared with that obtained by Liers et al (Li70).

Fig. 6 The differential scattering cross sections divided by the Rutherford cross section for the elastic scattering of protons from ^{66}Zn at 39.6MeV obtained in the present experiment are compared with that obtained by Liers et al (Li70).

Fig. 7 The differential scattering cross sections divided by the Rutherford cross section for the elastic scattering of protons from ^{68}Zn obtained in the present at 39.6MeV are compared with that obtained by Liers et al (Li70) at 39.6MeV and by Fricke et al (Fr67) at 40.0MeV.

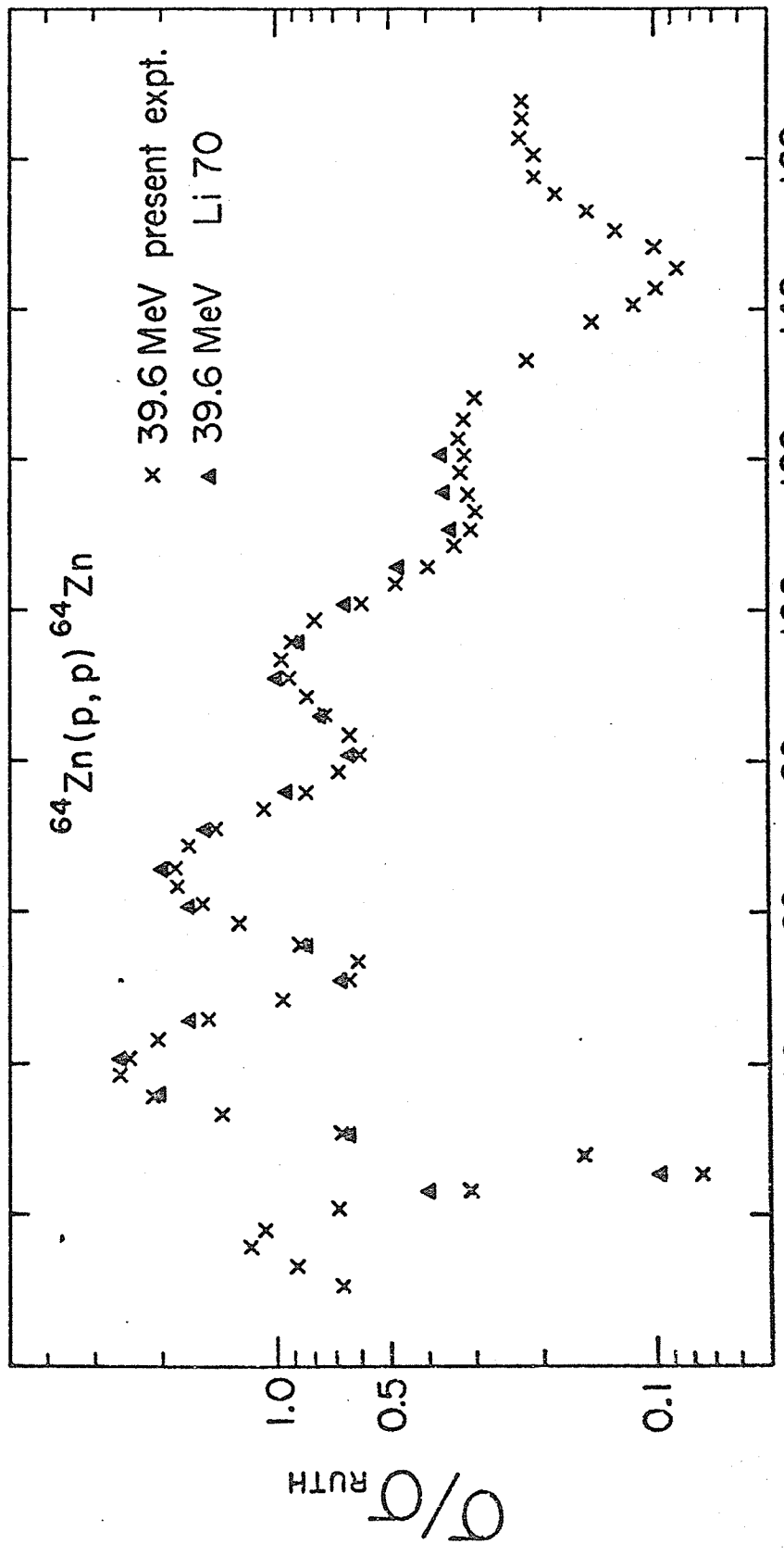
$^{64}Zn(p,p)^{64}Zn$
× 39.6 MeV present expt.
▲ 39.6 MeV Li 70
σ/σ_{RUTH}
1.0
0.5
0.1
20
40
60
80
100
120
140
160
$\theta_{c.m.}$ (degrees)

Fig. 5

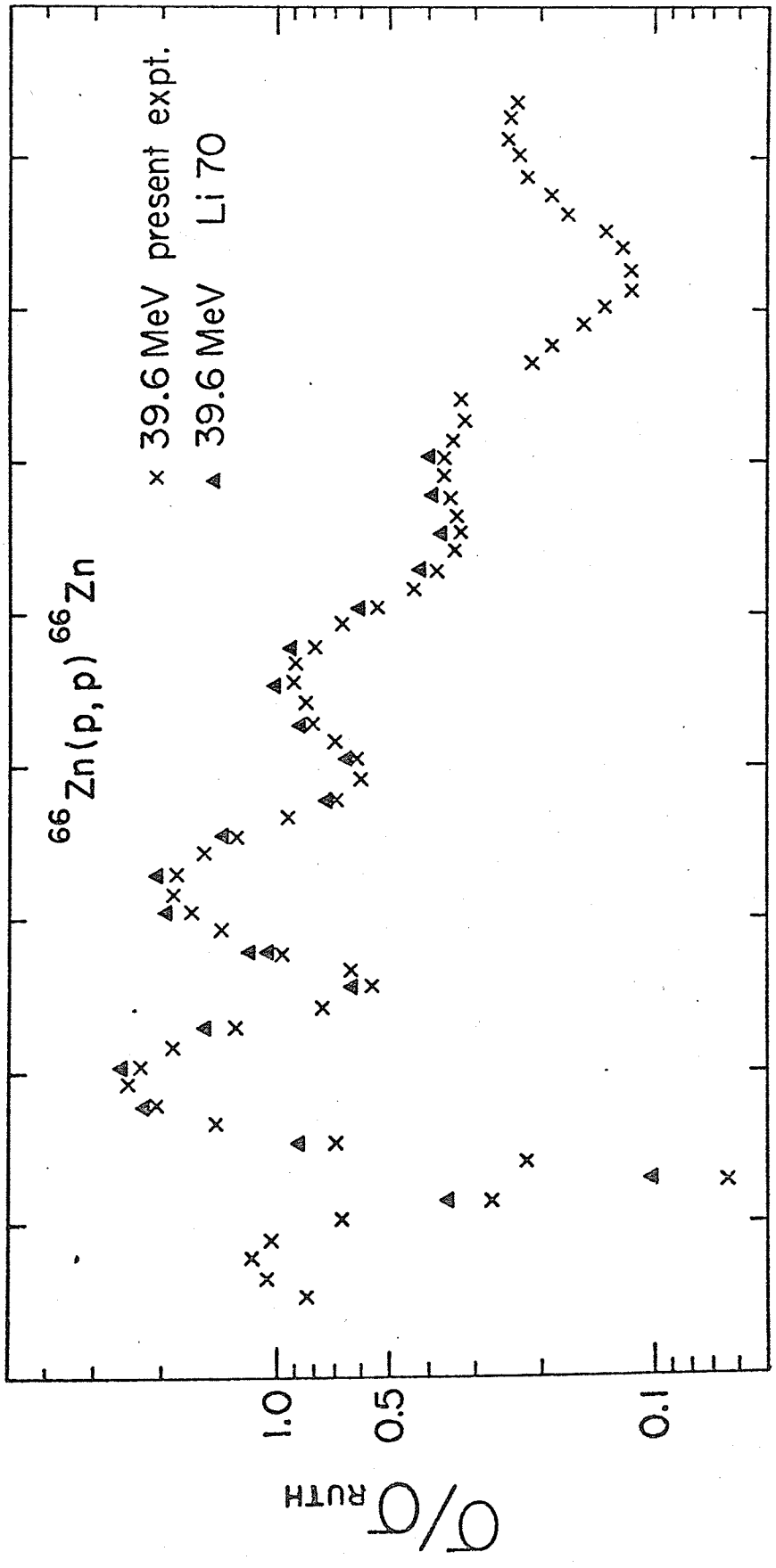
$^{66}Zn(p,p)^{66}Zn$
× 39.6 MeV present expt.
▲ 39.6 MeV Li 70
σ/σ_{RUTH}
1.0
0.5
0.1
20
40
60
80
100
120
140
160
$\theta_{c.m.}$ (degrees)

Fig. 6

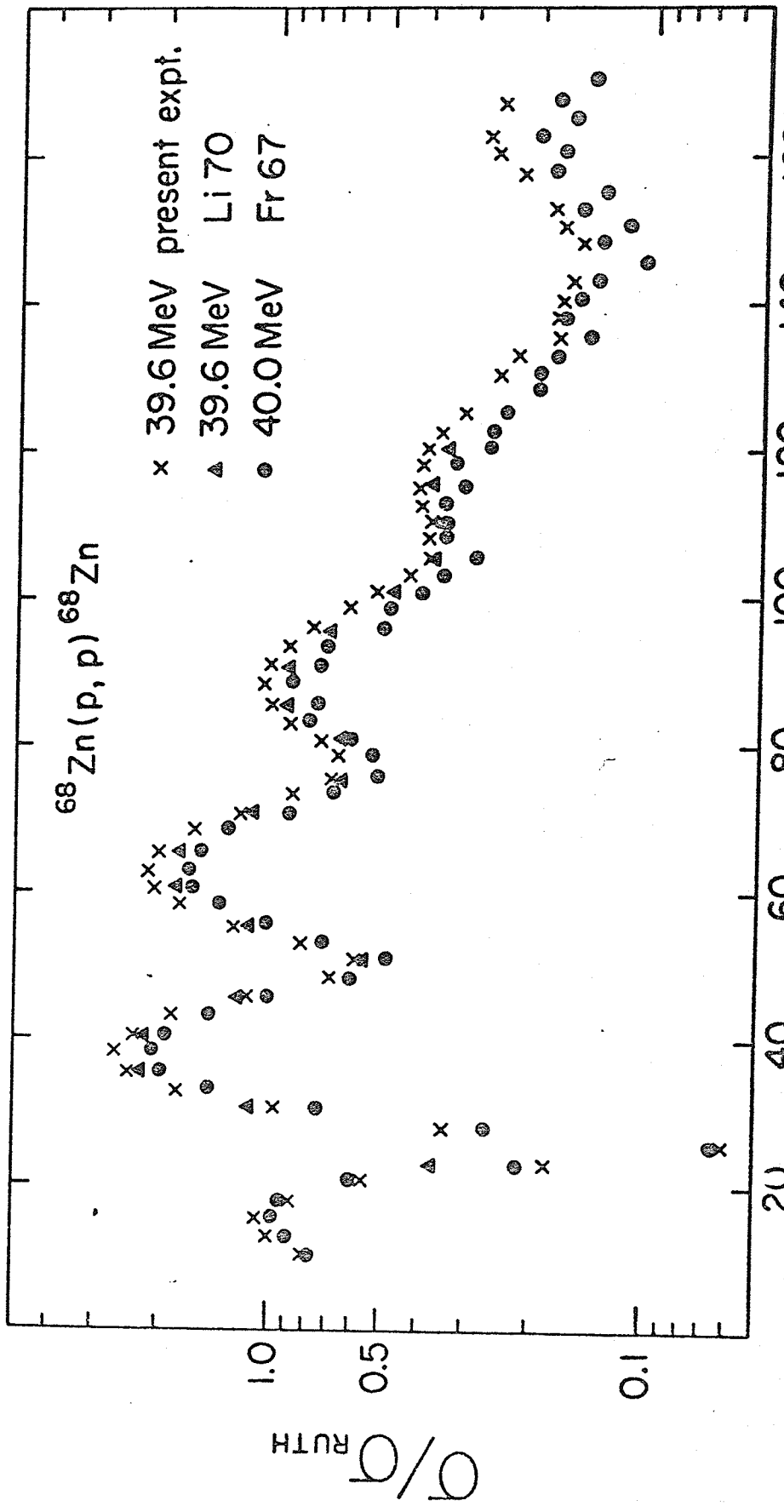
$^{68}Zn(p,p)^{68}Zn$
× 39.6 MeV present expt.
▲ 39.6 MeV Li 70
● 40.0 MeV Fr 67
σ/σ_{RUTH}
1.0
0.5
0.1
20
40
60
80
100
120
140
160
$\theta_{c.m.}$ (degrees)

Fig. 7

however, that the present data at 39.6MeV have more data points, cover a wider range of angles and show smoother angular distributions than those data obtained from the literature.

4.2 OPTICAL MODEL ANALYSIS

The analysis was performed by using the automatic search code SEEK (Me66) in a modified version which allows one to search for all 11 parameters in the optical model potential given by equation 3 in Chapter 2. Data included in the analysis are differential cross sections obtained in this experiment and differential cross sections and polarizations available in literature (see Table II). The 11 MeV data were normalized following Perey (Pe68). Existing best-fit parameters for the zinc isotopes or those for nearby isotopes or energies were used as starting values for the search. The value of the imaginary spin-orbit potential W_{so} was set to zero and not searched because it did not improve the fit appreciably in preliminary trial runs. During the initial fitting, searches were performed with the differential cross sections only so that the spin-orbit parameters V_{so} , r_{so} , and a_{so} were kept

Table II

Data included in the optical model analysis.

E_p	$d\sigma(\theta)/d\Omega$ (Ref)			$P(\theta)$ (Ref)		
(MeV)	^{64}Zn	^{66}Zn	^{68}Zn	^{64}Zn	^{66}Zn	^{68}Zn
11.00	Pe68*	Pe68*	Pe68*	Ro63**	Ro63**	Ro63**
14.50	Ke64	Ke64	Ke64	Ro63	Ro63	Ro63
22.20	EX	EX	EX	--	--	--
30.00	EX	EX	EX	--	--	--
39.60	EX	EX	EX	Li70	Li70	Li70
49.08	Ca67	Ca67	Ca67	Le67***	--	Le67****
61.40	--	--	Fu69	--	--	--

EX Present experiment

* Data were renormalized as done by Perey(Pe68).

** Data were measured at 10.5MeV.

*** Data were measured at 49.3MeV.

**** Data were measured at 49.5MeV.

fixed. When the differential cross sections were satisfactorily fitted the polarization data, if available, were then included in the fitting and all ten parameters searched.

For incident energies less than 30MeV, the value of the volume imaginary strength W was small and usually negative and did not improve the fit. Therefore it was set to be zero. On the other hand, when the data at 49.08MeV were fitted, the surface imaginary strength W_D became very small and it had no effect on the fit. For this reason W_D was fixed at zero for 49.08MeV and higher energies.

Table III lists the final optical model parameters and the corresponding theoretical total reaction cross sections. The final fit was selected mainly according to minimum χ^2, but in order to avoid false "best" fits, the parameters were also required to be either similar for all data sets or to follow a certain trend. The differential cross sections and polarizations with their theoretical fits are shown in Fig. 8 to 14.

As already mentioned in Chapter two, the parameters of the optical model are not unique. In order to avoid the ambiguities in

Table III

Optical model all parameters fits

r_c = 1.250fm

	E (MeV)	V (MeV)	r_o (fm)	a_o (fm)	W (MeV)	W_D (MeV)	r_I (fm)	a_I (fm)	V_{so} (MeV)	r_{so} (fm)	a_{so} (fm)	χ^2_σ	N_σ	N	χ^2_p	N_p	σ_R (mb)
^{64}Zn	11.00	46.74	1.289	0.749	0.0	12.74	1.393	0.446	-5.77	1.275	0.504	10.645	28	0.998	59.338	16	988.00
	14.50	48.29	1.266	0.663	0.0	13.92	1.324	0.423	-7.33	1.185	0.438	28.367	30	1.003	43.321	18	997.25
	22.20	50.83	1.190	0.723	0.0	10.50	1.275	0.518	-6.47	1.013	0.724	153.67	64	1.003	--	0	1131.9
	30.00	52.07	1.134	0.708	1.70	7.51	1.253	0.594	-6.51	1.146	1.048	324.94	63	1.004	--	0	1142.7
	39.60	47.13	1.147	0.770	5.44	2.06	1.405	0.623	-6.17	0.910	0.940	491.00	62	0.989	973.70	23	1158.2
	49.08	45.25	1.124	0.790	7.09	0.0	1.504	0.561	-6.43	1.014	0.774	1199.5	56	1.006	468.72	31	1090.8
^{66}Zn	11.00	52.24	1.245	0.645	0.0	8.31	1.227	0.679	-5.78	1.087	0.490	29.332	29	1.023	25.363	16	968.26
	14.50	47.92	1.279	0.689	0.0	16.38	1.341	0.375	-6.77	1.161	0.439	30.215	56	1.002	58.205	19	1023.6
	22.20	51.80	1.186	0.683	0.0	9.55	1.234	0.584	-6.32	1.002	0.661	103.63	64	1.005	--	0	1144.0
	30.00	53.05	1.123	0.719	1.91	7.15	1.258	0.632	-6.58	1.189	0.944	132.44	62	0.998	--	0	1197.4
	39.60	46.46	1.166	0.707	3.96	4.57	1.275	0.729	-7.67	0.879	0.989	307.38	63	1.008	127.23	23	1219.9
	49.08	45.11	1.121	0.764	6.87	0.0	1.521	0.567	-7.34	1.009	0.866	470.94	56	0.991	--	0	1120.2
^{68}Zn	11.00	46.24	1.332	0.669	0.0	15.40	1.345	0.414	-6.19	1.218	0.400	19.191	28	1.009	8.6741	16	982.92
	14.50	47.39	1.298	0.650	0.0	15.22	1.313	0.410	-6.92	1.067	0.580	38.766	31	1.003	57.151	19	1048.4
	22.20	50.26	1.212	0.606	0.0	9.00	1.247	0.604	-6.67	0.972	0.654	725.56	64	1.012	--	0	1165.7
	30.00	48.44	1.173	0.682	1.39	7.70	1.322	0.569	-7.38	1.196	0.820	836.31	58	0.980	--	0	1145.5
	39.60	45.33	1.188	0.704	2.95	4.83	1.260	0.741	-6.67	0.951	0.994	323.44	60	1.001	255.90	23	1239.2
	49.08	41.07	1.174	0.741	7.40	0.0	1.487	0.603	-5.91	1.035	0.738	1204.9	56	1.000	443.57	33	1156.8
	61.40	34.60	1.251	0.747	10.35	0.0	1.306	0.681	-3.47	1.078	0.717	67.590	41	1.001	--	0	1116.3

(N^{-1} is the normalization factor)

Fig. 8 The differential scattering cross sections divided by the Rutherford cross section for the elastic scattering of protons from ^{64}Zn at 11.0, 14.5, 22.2, 39.6, and 49.08 MeV. The experimental errors are comparable to the size of the dots unless indicated by error bars. The solid lines represent the "all-parameter" optical model fits.

Fig. 9 The differential scattering cross sections divided by the Rutherford cross section for the elastic scattering of protons from ^{66}Zn at 11.0, 14.5, 22.2, 39.6, and 49.08 MeV. The experimental errors are comparable to the size of the dots unless indicated by error bars. The solid lines represent the "all-parameter" optical model fits.

Fig. 10 The differential scattering cross sections divided by the Rutherford cross section for the elastic scattering of protons from ^{68}Zn at 11.0, 14.5, 22.2, 39.6, 49.08, and 61.4 MeV. The experimental errors are comparable to the size of the dots unless indicated by error bars. The solid lines represent the "all-parameter" optical model fits.

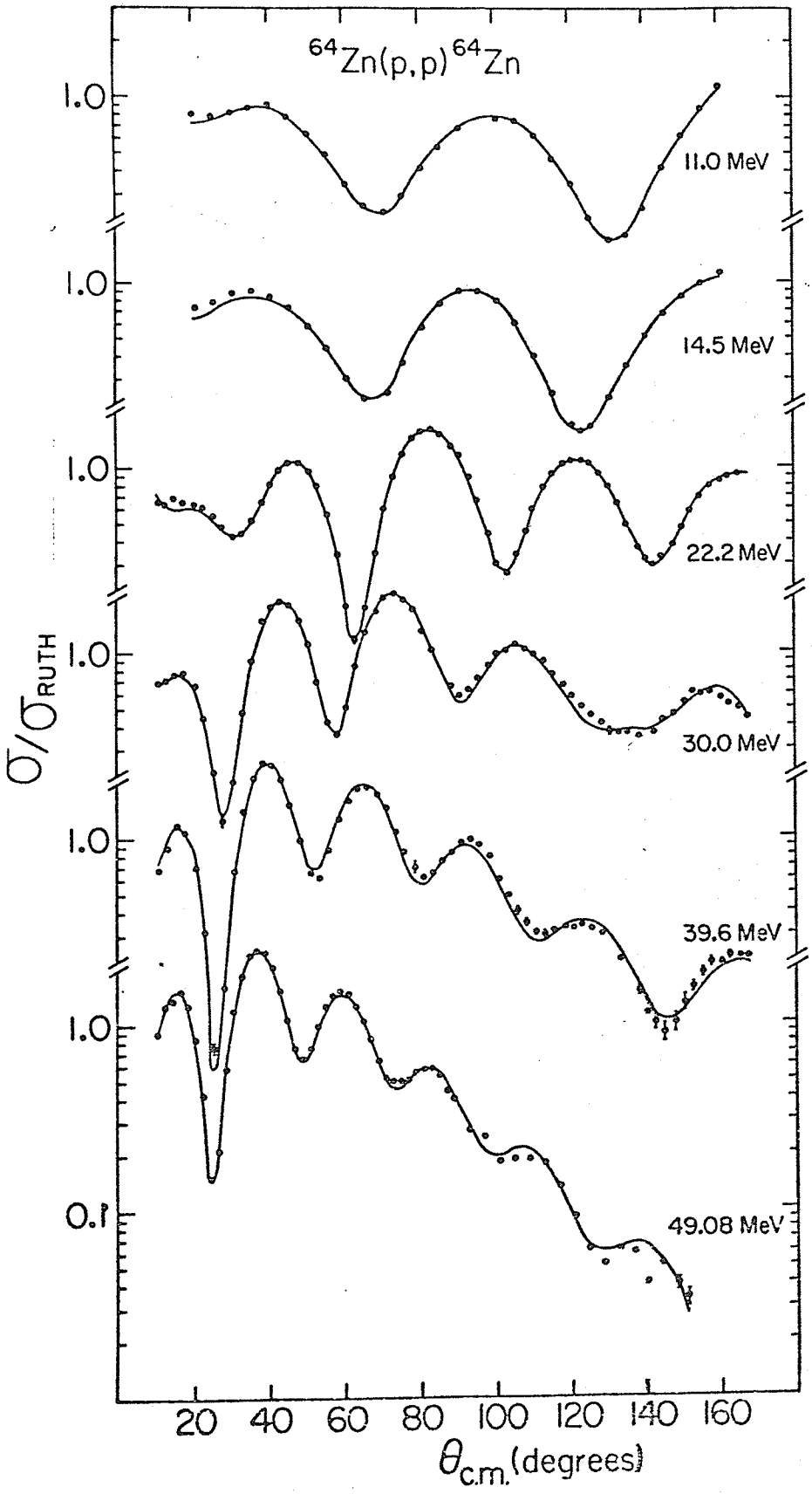
$^{64}Zn(p,p)^{64}Zn$
11.0 MeV
14.5 MeV
22.2 MeV
30.0 MeV
39.6 MeV
49.08 MeV
1.0
1.0
1.0
1.0
1.0
0.1
σ/σ_{RUTH}
20
40
60
80
100
120
140
160
$\theta_{c.m.}$ (degrees)

Fig. 8

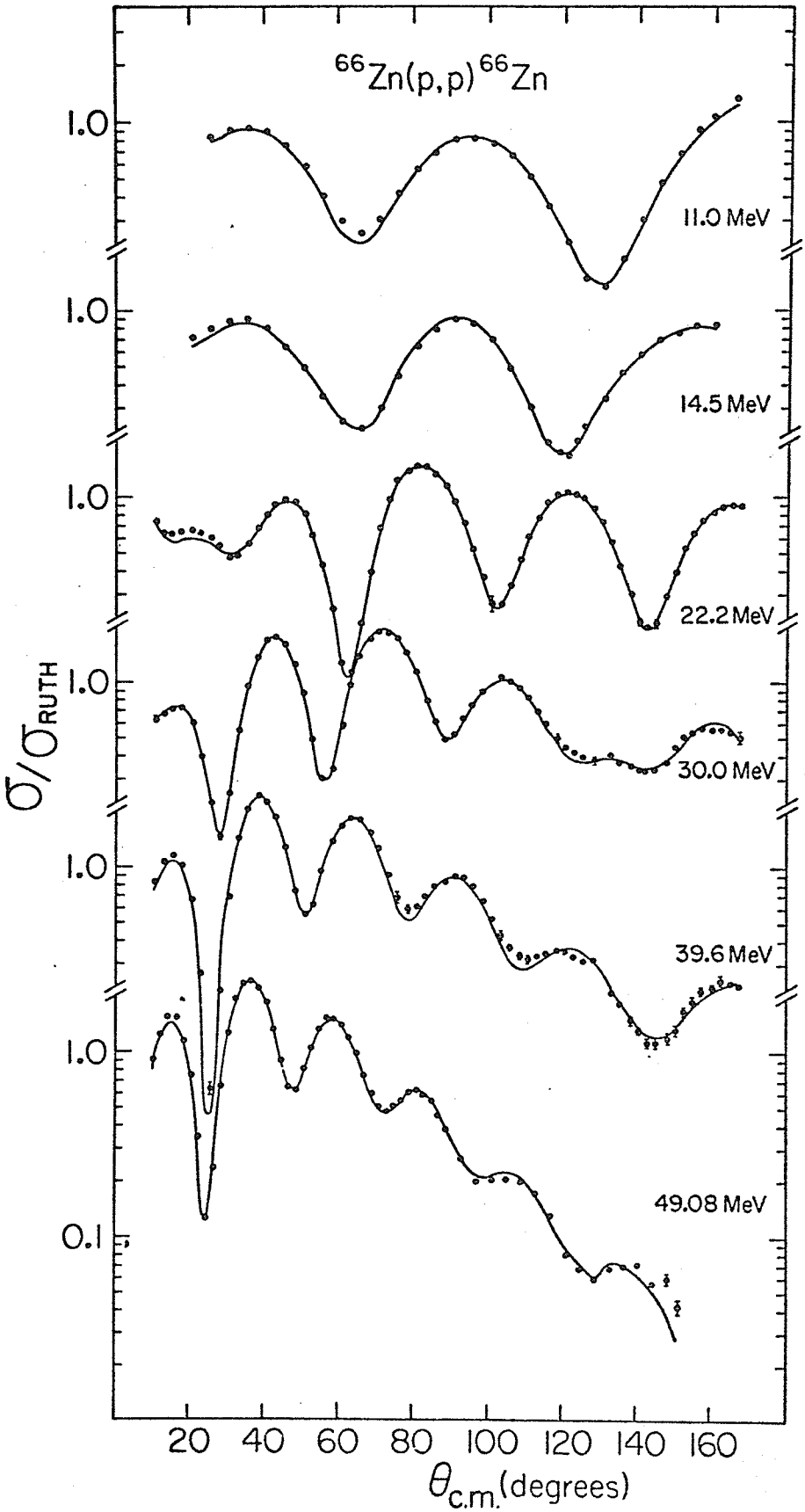
$^{66}Zn(p,p)^{66}Zn$
11.0 MeV
14.5 MeV
22.2 MeV
30.0 MeV
39.6 MeV
49.08 MeV
1.0
0.1
σ/σ_{RUTH}
20 40 60 80 100 120 140 160
$\theta_{c.m.}$(degrees)

Fig. 9

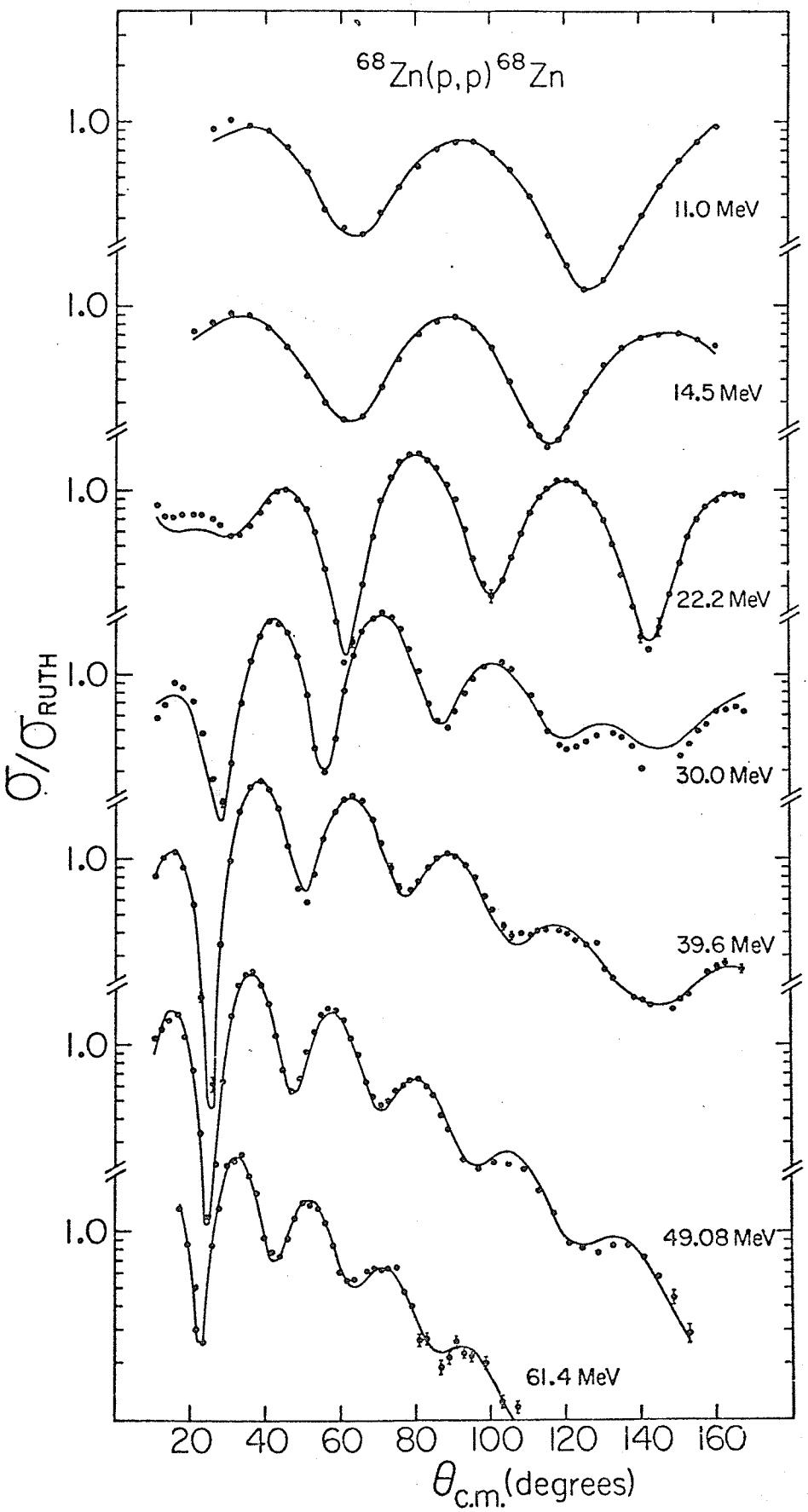
$^{68}Zn(p,p)^{68}Zn$
1.0
11.0 MeV
14.5 MeV
22.2 MeV
30.0 MeV
39.6 MeV
49.08 MeV
61.4 MeV
σ/σ_{RUTH}
20 40 60 80 100 120 140 160
$\theta_{c.m.}$(degrees)

Fig. 10

Fig. 11 Polarizations for the elastic scattering of protons from ^{64}Zn, ^{66}Zn, and ^{68}Zn at 10.5MeV. The experimental errors are comparable to the size of the dots unless indicated by error bars. The solid lines represent the "all-parameter" optical model fits at 11.0MeV.

Fig. 12 Polarizations for the elastic scattering of protons from ^{64}Zn, ^{66}Zn, and ^{68}Zn at 14.5MeV. The experimental errors are comparable to the size of the dots unless indicated by error bars. The solid lines represent the "all-parameter" optical model fits.

Fig. 13 Polarizations for the ealstic scattering of protons from ^{64}Zn, ^{66}Zn, and ^{68}Zn at 39.6MeV. The experimental errors are comparable to the size of the dots unless indicated by error bars. The solid lines represent the "all-parameter" optical model fits.

Fig. 14 Polarizations for the elastic scattering of protons from ^{64}Zn at 49.3MeV and ^{68}Zn at 49.5MeV. The experimental errors are comparable to the size of the dots unless indicated by error bars. The solid lines represent the "all-parameter" optical model fits at 49.08MeV.

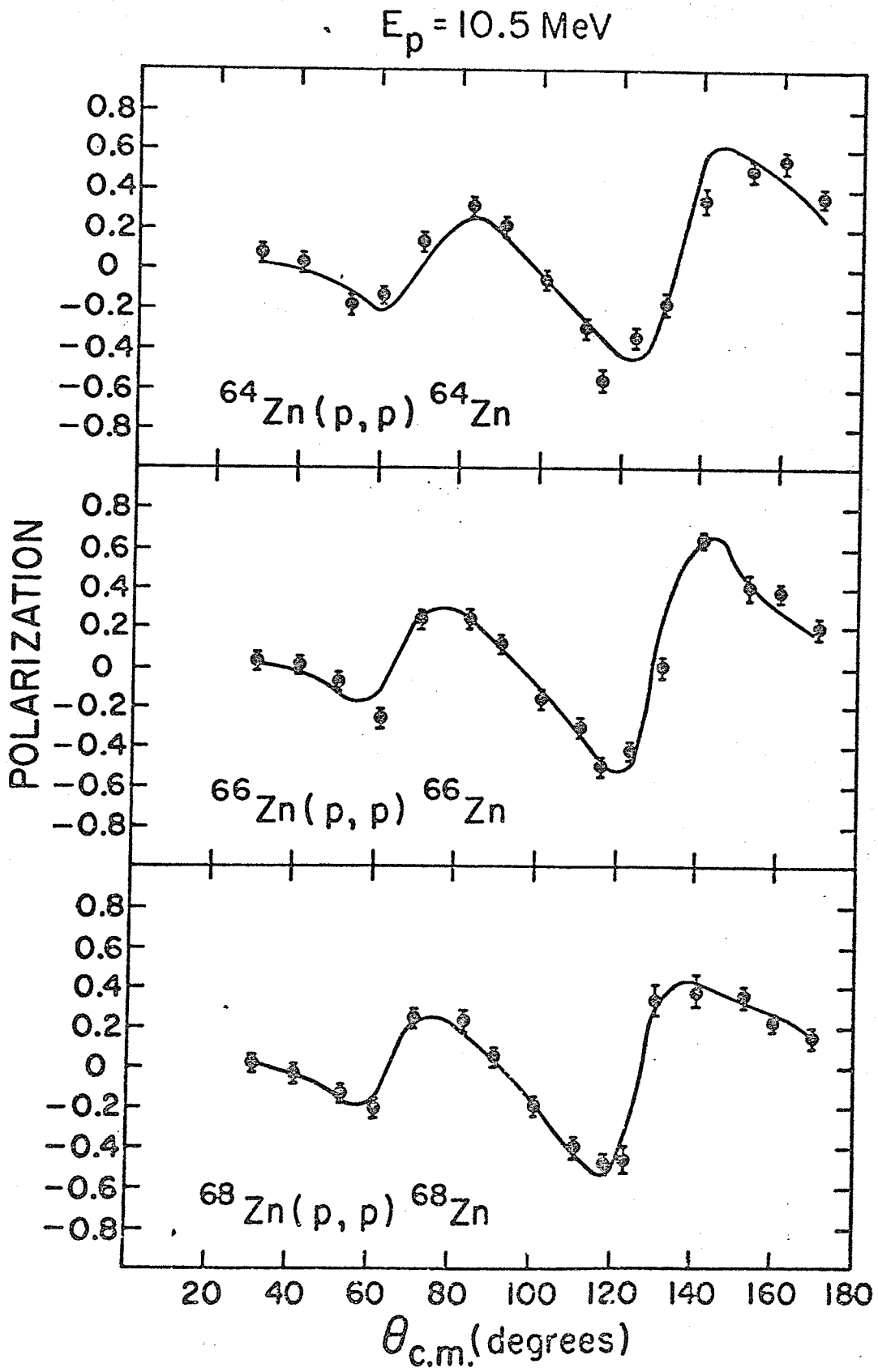
E_p = 10.5 MeV
POLARIZATION
^{64}Zn(p, p) ^{64}Zn
^{66}Zn(p, p) ^{66}Zn
^{68}Zn(p, p) ^{68}Zn
0.8
0.6
0.4
0.2
0
−0.2
−0.4
−0.6
−0.8
20
40
60
80
100
120
140
160
180
$\theta_{c.m.}$(degrees)

Fig. 11

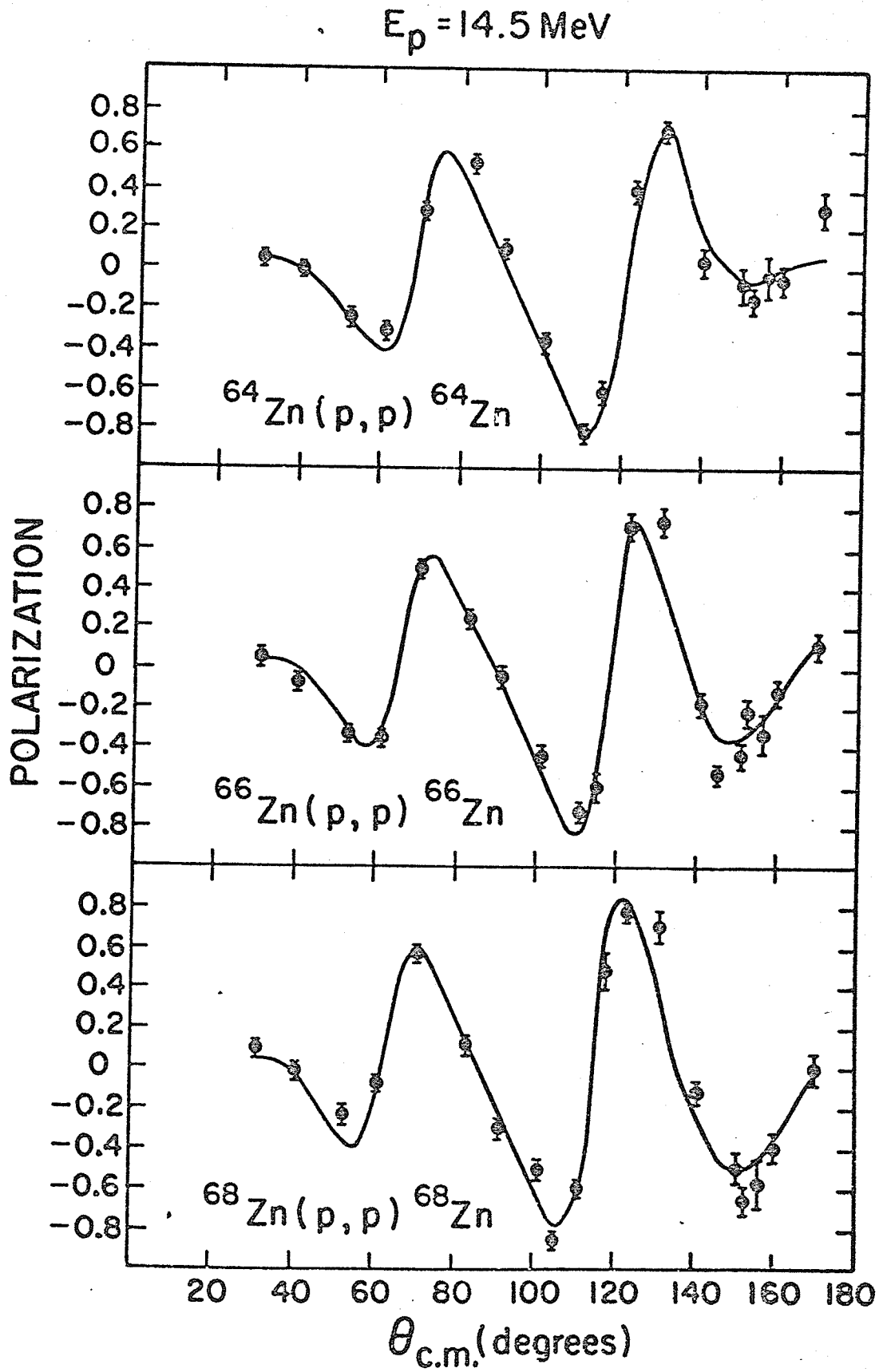
$E_p = 14.5$ MeV
POLARIZATION
$^{64}Zn(p,p)^{64}Zn$
$^{66}Zn(p,p)^{66}Zn$
$^{68}Zn(p,p)^{68}Zn$
0.8
0.6
0.4
0.2
0
-0.2
-0.4
-0.6
-0.8
20
40
60
80
100
120
140
160
180
$\theta_{c.m.}$ (degrees)

Fig. 12

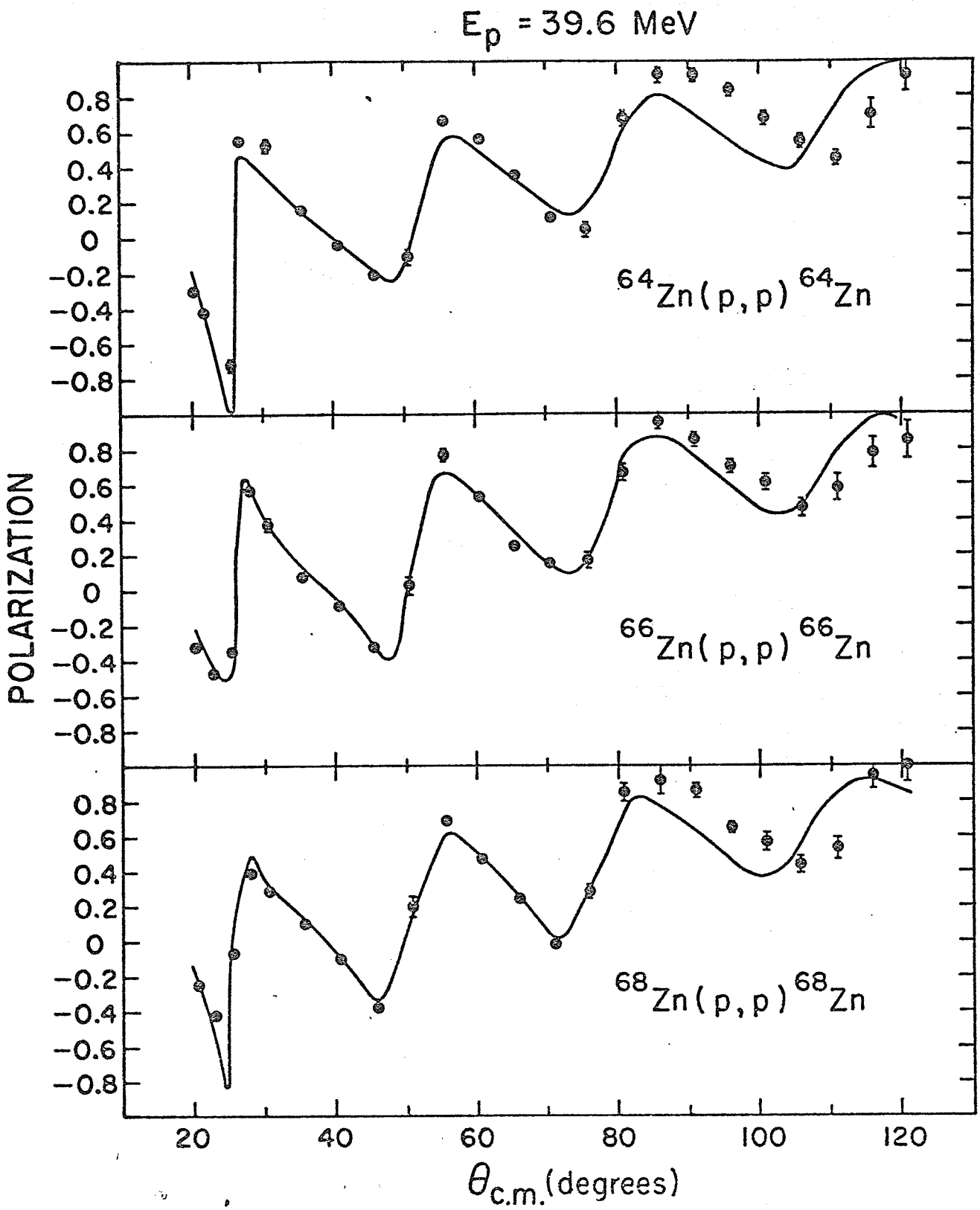
E_p = 39.6 MeV
POLARIZATION
^{64}Zn(p,p)^{64}Zn
^{66}Zn(p,p)^{66}Zn
^{68}Zn(p,p)^{68}Zn
0.8
0.6
0.4
0.2
0
-0.2
-0.4
-0.6
-0.8
20
40
60
80
100
120
$\theta_{c.m.}$(degrees)

Fig. 13

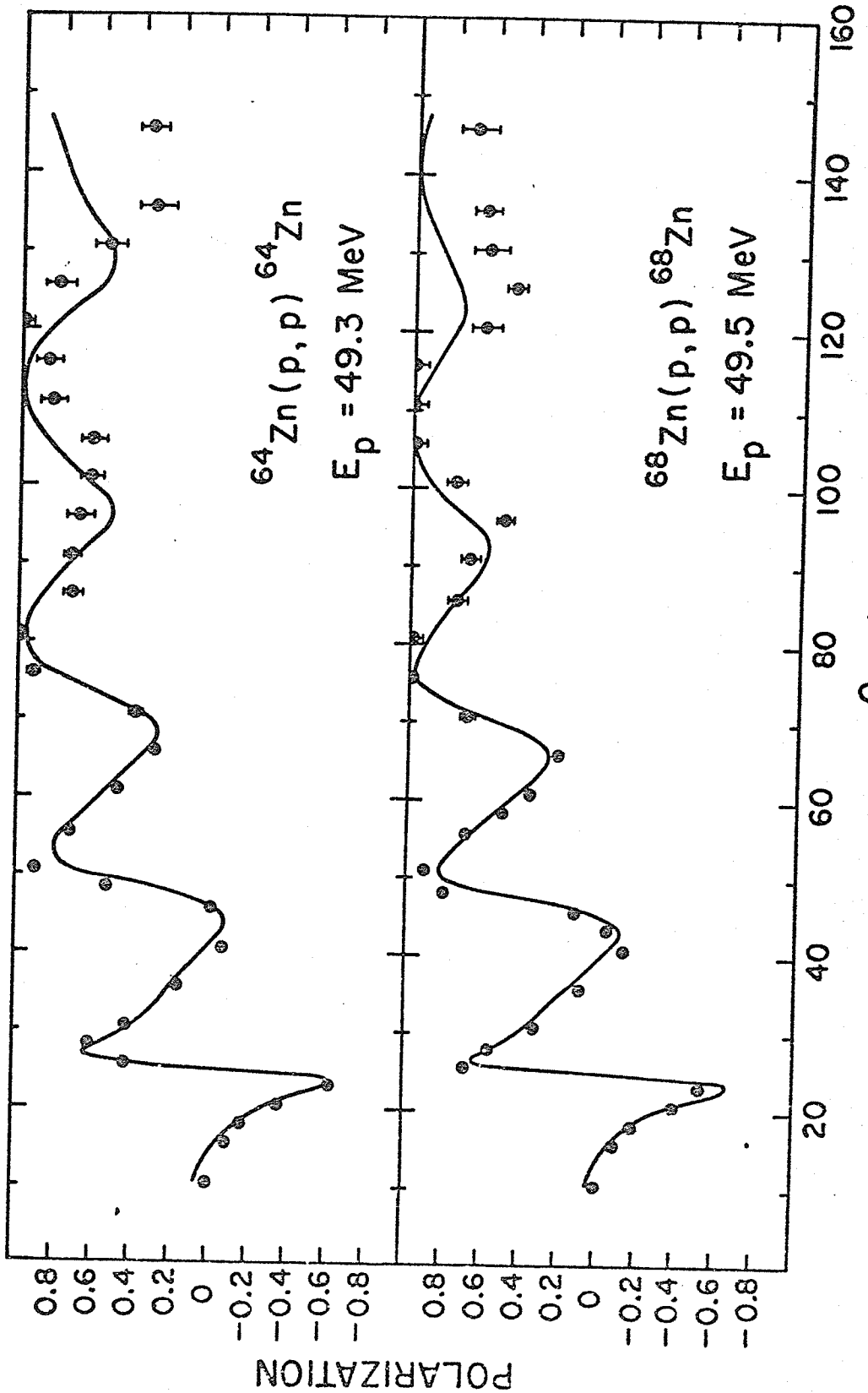
$^{64}Zn(p,p)^{64}Zn$
$E_p = 49.3$ MeV
$^{68}Zn(p,p)^{68}Zn$
$E_p = 49.5$ MeV
POLARIZATION
$\theta_{c.m.}$(degrees)
0.8
0.6
0.4
0.2
0
-0.2
-0.4
-0.6
-0.8
20
40
60
80
100
120
140
160

Fig. 14

parametrization, common geometric parameters were obtained by averaging the best fit values, and the potential strength parameters were again searched with the common geometric parameters fixed. This approach is justified because the geometric parameters do not show any systematic dependence on incident energy or on the constitution of target nuclei.

By averaging the best fit geometric parameters in Table III, the following set of common values was obtained:

r_o = 1.205fm. r_I = 1.331fm. r_{so} = 1.073fm.

a_o = 0.706fm. a_I = 0.566fm. a_{so} = 0.722fm.

One may notice that this set of common geometric parameters is quite close to that given by Becchetti (p.14). With this set of geometric parameters, the four potential strength parameters V, W, W_D, and V_{so} were searched. W was fixed at zero for data below 20MeV while W_D was fixed at zero for the 61.4MeV data. The resulting numerical values for the various potential strengths are listed in Table IV. As the fit for ^{68}Zn at 22.2MeV was comparatively worse at the forward angles, optical model fitting was also performed not including data points above 120° and again above 90° . The results were not given in Table IV because the fit at forward angles was not improved significantly.

Table IV
Optical model parameters with fixed geometry

r_c = 1.250fm
r_o = 1.205fm r_I = 1.331fm r_{so} = 1.073fm
a_o = 0.706fm a_I = 0.566fm a_{so} = 0.722fm

	E (MeV)	V (MeV)	W (MeV)	W_D (MeV)	V_{so} (MeV)	χ^2_σ	N_σ	N	χ^2_p	N_p
^{64}Zn	11.00	53.37	0.0	9.31	-5.76	134.77	28	0.968	60.553	16
	14.50	51.04	0.0	9.36	-7.14	320.86	30	0.993	56.305	18
	22.20	48.28	2.14	6.96	-7.20	1954.0	64	1.010	--	0
	30.00	45.56	2.61	5.99	-5.32	3584.0	63	0.976	--	0
	39.60	43.46	4.92	4.00	-5.14	1262.5	62	0.976	1113.4	23
	49.08	39.64	5.56	3.57	-5.34	4191.7	56	0.970	598.50	31
^{66}Zn	11.00	54.20	0.0	9.31	-5.76	76.508	29	1.019	28.214	16
	14.50	51.37	0.0	9.49	-6.97	241.50	56	0.981	110.07	19
	22.20	48.38	3.25	6.20	-6.80	2670.7	64	1.013	--	0
	30.00	46.23	3.04	6.12	-6.00	3583.5	62	0.972	--	0
	39.60	43.47	5.43	3.79	-4.99	1639.1	63	0.976	624.44	23
	49.08	39.43	5.87	3.27	-5.14	3126.3	56	0.970	--	0
^{68}Zn	11.00	54.18	0.0	9.46	-4.83	118.48	28	0.946	18.916	16
	14.50	51.73	0.0	9.82	-6.68	214.28	31	0.968	100.10	19
	22.20	47.96	2.88	6.47	-5.78	4136.0	64	1.034	--	0
	30.00	46.45	1.43	7.41	-6.16	1900.8	58	0.997	--	0
	39.60	44.54	3,81	4.91	-4.62	1743.4	60	0.976	508.20	23
	49.08	39.23	6.84	2.94	-5.62	3164.0	56	0.978	489.80	33
	61.40	38,87	11.96	0.0	-4.34	531.79	41	0.983	--	0

(N^{-1} is the normalization factor)

4.3 DISCUSSION

It can be noticed in Table IV that, for 11MeV, 14.5MeV and 22.2MeV, the surface imaginary potential increases very slowly but consistently with energy. When the volume imaginary potential was included in the search routine, the surface imaginary potential decreased rapidly with energy while the volume imaginary potential increased rapidly. This is in accord with the fact that, as mentioned in section 2.1, absorption takes place throughout the whole nucleus for high energy. The real central potential seems to depend linearly on E and $\frac{N-Z}{A}$. In order to find out how the energy dependence changes from one isotope to another, a linear least squares fit to V was first performed as a function of proton energy. The error in the real central potential strength used in the fitting was obtained according to the following procedure. "Fixed common geometry" optical model fittings were examined for each data set. The change in V for 10% change of χ^2 was taken to be the error in V. Although W, W_D, and V_{so} were also variables in the fittings, the possible effect on V caused by variation in W, W_D, and V_{so} was not considered explicitly because their correlations

are quite complicated and very little was known about them. The slopes dV/dE for the three isotopes ^{64}Zn, ^{66}Zn and ^{68}Zn are listed in Table V. It can be seen that, within errors, dV/dE is the same for the three isotopes studied.

In order to obtain the isospin dependence of V linear least squares fits were also obtained for V vs $\frac{N-Z}{A}$ for each incident energy. The resulting expressions are given in Table VIa. As there are only three points to determine each relationship, it is not surprising to see the values of $dV/d(\frac{N-Z}{A})$ not being consistent from one energy to another. Consequently, the values in Table VIa may not represent the isospin dependence of the real potential accurately. A simultaneous search of all available data was therefore performed to find the energy dependence and isospin dependence for all 19 values of the real potential at different energies for the 3 isotopes. This is justified because the energy dependence of the zinc isotopes are almost the same (see Table V). The real potentials were fitted to the formula

$$V = V_0 - \gamma E + U_1 \frac{N-Z}{A} + 0.4 \frac{Z}{A^{1/3}}.$$

The best fit values are given in Table VIb.

The above "common geometry" approach was used extensively before the reformulated optical

TABLE V

	ENERGY RANGE (MeV)	dV/dE	ENERGY RANGE (MeV)	dV/dE
^{64}Zn	10 - 50	-0.329±0.007	20 - 50	-0.321±0.009
^{66}Zn	10 - 50	-0.344±0.004	20 - 50	-0.334±0.004
^{68}Zn	10 - 60	-0.356±0.006	20 - 50	-0.342±0.009

TABLE VI

ENERGY (MeV)	$dV/d\frac{N-Z}{A}$ (MeV)
11.00	14.9±12.8
14.50	12.5±7.7
22.20	-4.1±5.7
30.00	15.2±12.8
39.60	19.2±7.1
49.08	-7.5±3.1

Simultaneous search for energy dependence and isospin dependence

	all 19 data sets	20MeV<E< 50MeV
V_o	53.46±0.23	53.14±0.26
γ	-0.344±0.003	-0.333±0.003
U_1	-1.0±2.3	-3.8±2.5

model (Gr68) was proposed. Although good results were obtained, the common geometry approach is not without ambiguity. The values of common geometric parameters do depend slightly on the data sets used and the use of common geometry worsens the fit. Therefore the possible errors in the potential strength parameters are much larger. The introduction of the reformulated optical model provided a different approach to the study of the optical model. Greenlees et al (Gr68) suggested that the mean square radius $\langle r^2 \rangle$ and the volume integral J of the real central potential should be used to study the real central potential because they seem to be quite well defined in the optical model analysis. These two quantities are defined as

$$J = \int V(\bar{r})\, d\bar{r}$$

$$\langle r^2 \rangle = \frac{\int r^2 V(\bar{r})\, d\bar{r}}{\int V(\bar{r})\, d\bar{r}}.$$

Taking the form factor to be Woods-Saxon, they can be simplified to

$$J = \frac{4\pi}{3} V R^3 \left(1+\frac{\pi^2 a_o^2}{R^2}\right)$$

$$\langle r^2 \rangle = \frac{1}{5} \left(3R^2+7\pi^2 a_o^2\right)$$

where $R = r_o A^{1/3}$ and a_o is the diffuseness parameter. Plots of J/A vs E and $\langle r^2 \rangle^{1/2}$ vs E for ^{64}Zn, ^{66}Zn,

Fig. 15 The rms radius and the volume integral per nucleon of the real central optical model potential for ^{64}Zn plotted versus the incident proton energy for the range 10-50MeV. The solid line represent linear fits to the volume integrals per nucleon according to the relation $J/A = J_o/A + \alpha_1 E$ for E between 20 and 50 MeV.

Fig. 16 The rms radius and the volume integral per nucleon of the real central optical model potential for ^{66}Zn plotted versus the incident proton energy for the range 10-50MeV. The solid line represent linear fits to the volume integrals per nucleon according to the relation $J/A = J_o/A + \alpha_1 E$ for E between 20 and 50 MeV.

Fig. 17 The rms radius and the volume integral per nucleon of the real central optical model potential for ^{68}Zn plotted versus the incident proton energy for the range 10-60MeV. The solid line represent linear fits to the volume integrals per nucleon according to the relation $J/A = J_o/A + \alpha_1 E$ for E between 20 and 50 MeV.

(The errors in the rms radii and the volume integral per nucleon of the real central optical potential were taken to be the corresponding changes with 10% change in χ^2 as mentioned previously. Wherever error bar is not shown the error is less than the size of the dots.)

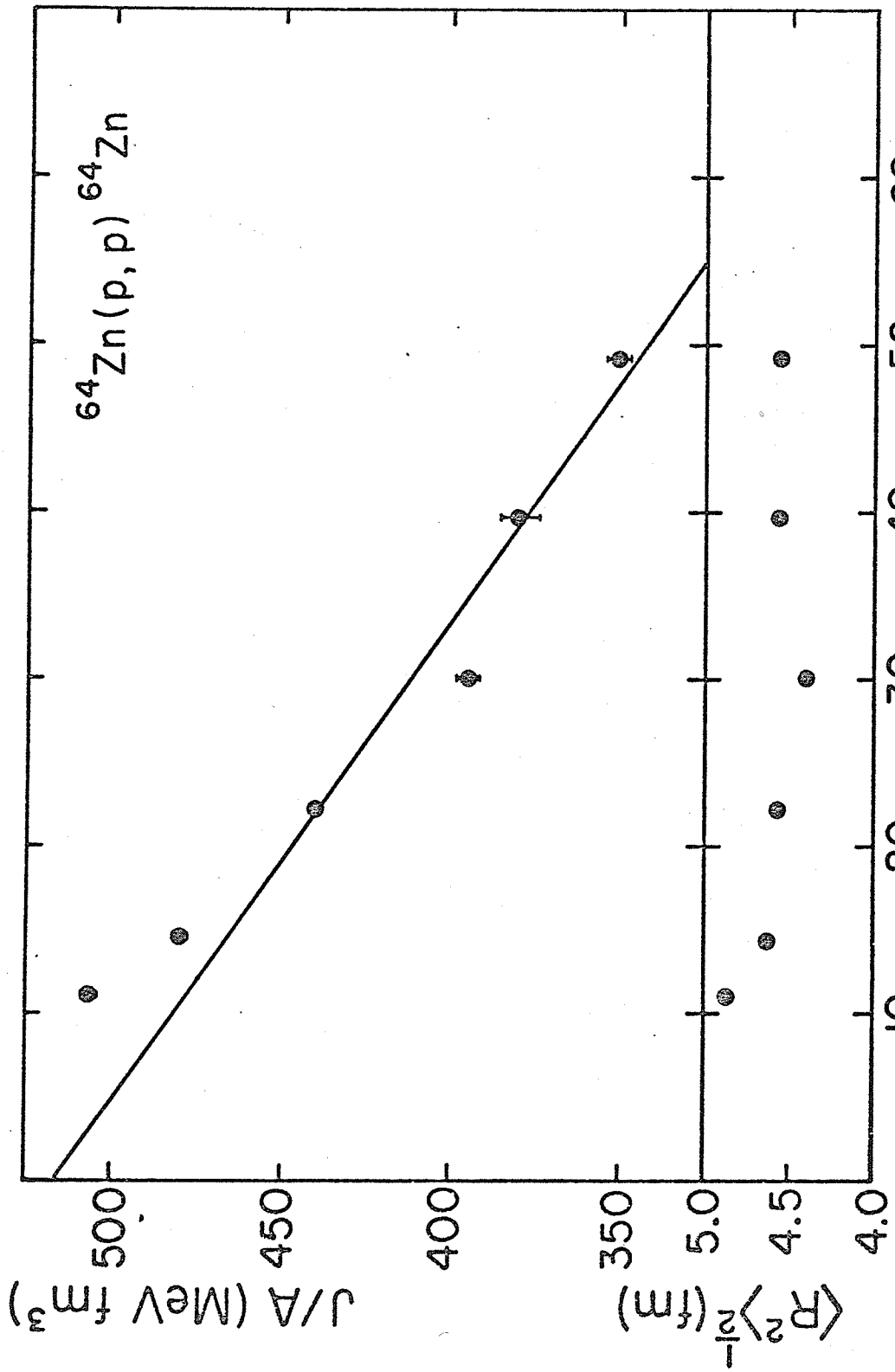
$^{64}Zn(p,p)^{64}Zn$
J/A (MeV fm^3)
$\langle R^2 \rangle^{\frac{1}{2}}$ (fm)
E_p (MeV)
500
450
400
350
5.0
4.5
4.0
10
20
30
40
50
60

Fig. 15

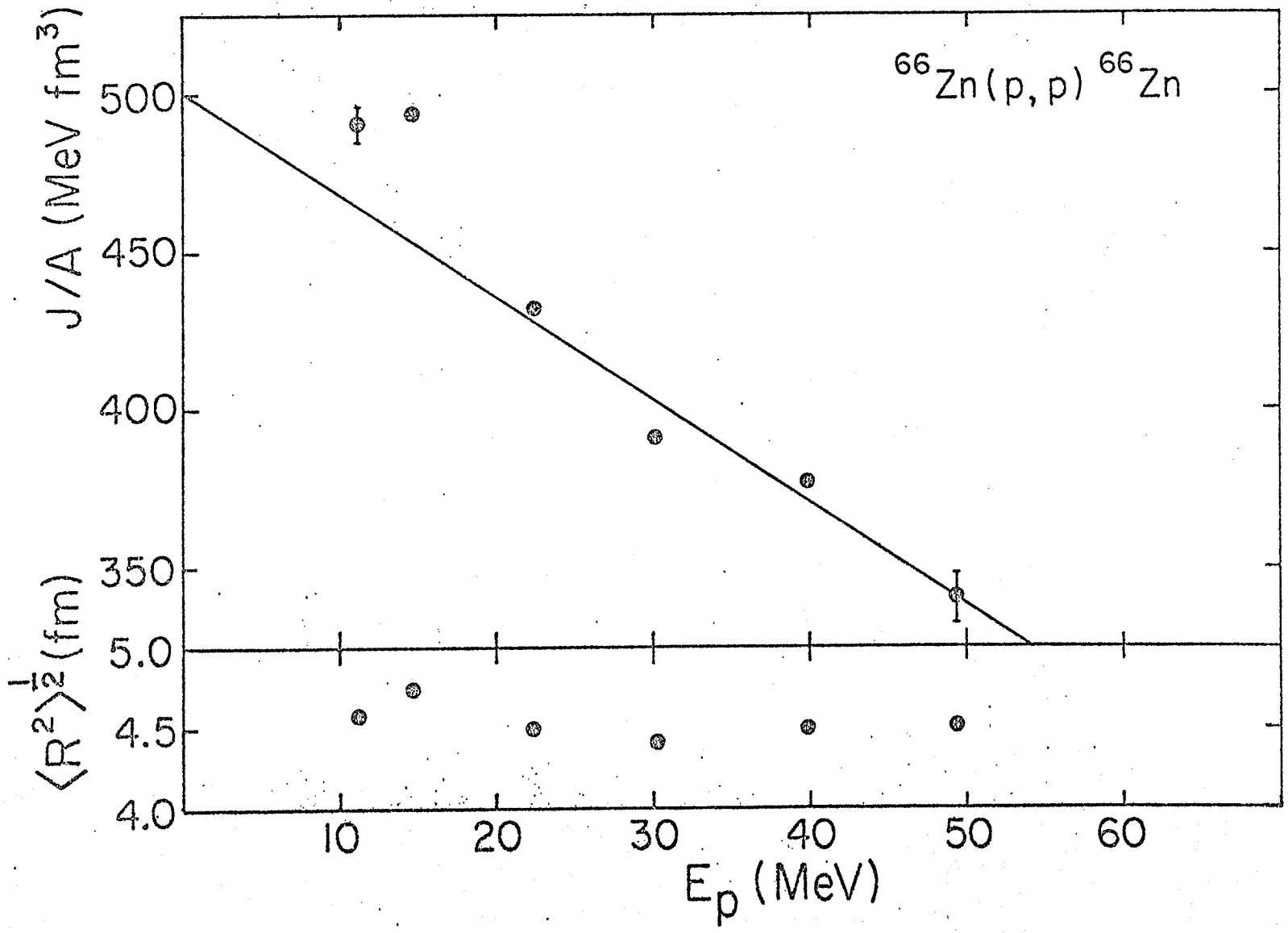
^{66}Zn(p, p) ^{66}Zn
J/A (MeV fm^3)
500
450
400
350
$\langle R^2 \rangle^{\frac{1}{2}}$ (fm)
5.0
4.5
4.0
10
20
30
40
50
60
E_p (MeV)

Fig.16

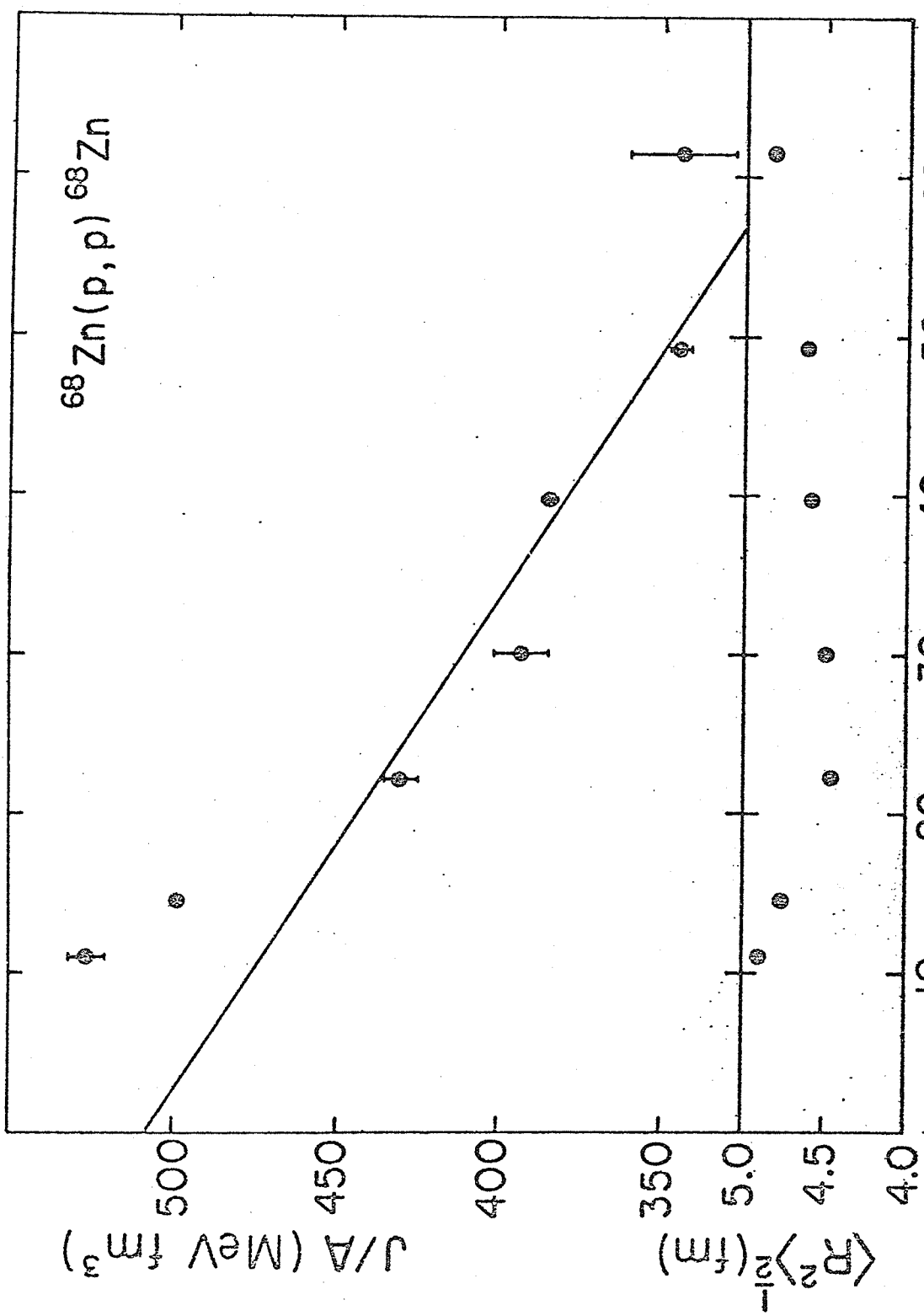
$^{68}Zn(p,p)^{68}Zn$
E_p (MeV)
$\langle R^2 \rangle^{\frac{1}{2}}_{\pi l}$ (fm)
J/A (MeV fm^3)
4.0
4.5
5.0
350
400
450
500
10
20
30
40
50
60

Fig. 17

and ^{68}Zn are shown in Fig.15 to 17. These graphs show that, for E greater than 20MeV, the volume integral per nucleon decreases with energy linearly while the root mean square radius stays constant with energy. When E is below 20MeV, the volume integral per nucleon and root mean square radius rapidly move above the linear relationship with energy as the energy decreases. This behaviour of the volume integral per nucleon and root mean square radius has also been observed for other isotopes (Hu72). This could be related to the fact that effects due to core polarization and exchange become important at low energies (Ma72). The volume integrals per nucleon for energies above 20MeV were fitted to

$$J/A = J_o/A + \alpha_1 E_p$$

for the three zinc isotopes separately. Error in the volume integral was again obtained from the change of J corresponding to 10% change of χ^2 as done previously. The values of α_1 obtained are listed in Table VII. Also shown in Table VII are the average root mean square radii (11MeV and 14.5MeV not included) for ^{64}Zn, ^{66}Zn, and ^{68}Zn as well as α_1 and $\langle r^2 \rangle^{1/2}$ for ^{6}Li, ^{16}O, ^{40}Ca, and ^{208}Pb obtained by others. It is apparent that although the values of $\frac{d(J/A)}{dE}$ for the zinc

isotopes are consistent among themselves, they are in disagreement with the results for ^{40}Ca and ^{208}Pb. It can be noted that these two isotopes have both neutron and proton shells closed, but there is no obvious reason why this should cause the value of $\frac{d(J/A)}{dE}$ to differ from that for other nuclei.

Greenless et al (Gr68) showed that the volume integral should also depend on the isospin according to

$$J/A = J_d (1+\zeta\frac{N-Z}{A})$$

Unfortunately this could not be examined accurately in the present study as only three isotopes were studied. The values of ζ (see Table VIII) for each energy scatter between 1 and -0.5, and it is very hard to say what the most probable value is. As the energy dependence of the volume integral per nucleon between 20MeV and 50MeV was almost the same for all the zinc isotopes, the volume integral per nucleon in that energy range were fitted using the formula

$$J/A = J_d (1+\zeta'\frac{N-Z}{A}) + \alpha_1 E + 2.36\frac{Z}{A^{\frac{1}{3}}}$$

The best fit values were

$$J_d = 499.3 \pm 2.6$$

$$\alpha_1 = -3.228 \pm 0.062$$

$$\zeta' = -0.300 \pm 0.062$$

It is obvious that the value obtained for ζ' is

TABLE VII

	ENERGY RANGE (MeV)	$\frac{dJ/A}{dE}$ (fm^3)	$\langle r^2 \rangle^{1/2}$ (fm)	ref
^{6}Li	25 - 50	-4.25		Lo70
^{16}O	25 - 100	-3.80±0.50	3.51±0.05	Va69
^{40}Ca	25 - 180	-2.16±0.07	4.05±0.03	Va71
^{64}Zn	20 - 50	-3.45±0.11	4.52±0.09	
^{66}Zn	20 - 50	-3.24±0.08	4.48±0.04	
^{68}Zn	20 - 50	-3.24±0.22	4.59±0.08	
^{208}Pb	25 - 180	-1.95±0.03	6.04±0.04	Va74

TABLE VIII

Energy (MeV)	ς
11.00	0.48±0.19
14.50	0.72±0.11
22.20	-0.46±0.10
30.00	-0.14±0.26
39.60	0.62±0.21
49.08	-0.36±0.21

much lower than the value $\zeta = 0.48$ estimated by Greenlees(Gr68) using the soft core potential proposed by Tang et al (Ta63). Low values of ζ have usually been obtained for the isospin dependence in studies done previously using volume integral per nucleon (Si72). The possible reason for this is the neglect of second and higher order terms arising predominantly from the tensor force. Another obvious reason is the factor $(1+\frac{\pi^2 a_o^2}{r_o^2 A^{2/3}})$ which decreases with the increase in mass number when a_o and r_o are considered to be constant. In the case of the zinc isotopes the factor $(1+\frac{\pi^2 a_o^2}{r_o^2 A^{2/3}})$ decreases by 0.5% from ^{64}Zn to ^{66}Zn (also for ^{66}Zn to ^{68}Zn). The isospin dependent term in

$$V = V_o - \alpha E + U_1 \frac{N-Z}{A} + 0.4\frac{Z}{A^{1/3}}$$

would cause an increase of 1.2% if the isospin potential strength U_1 is taken to be 24MeV. As the isospin potential strength was found to be almost zero for the zinc isotopes when "common geometry" potential for $20MeV < E < 50MeV$ was used (see Table VI), it is not at all surprising to see that a negative value for the isospin dependence was obtained using volume integral per nucleon.

The large difference in the isospin dependence obtained for the zinc isotopes compared with accepted values for U_1 and ζ suggests that a

nuclear structure effect neglected in this analysis may be important in the case of zinc isotopes. However, as already mentioned in Chapter Two, neither change of shell for the outermost nucleons nor drastic change of deformation seem to be applicable to the zinc isotopes. There may be some details of structure of the zinc nuclei that must be discovered in order to explained this anomaly among the zinc isotopes but at present the origin of the anomalously small isospin dependence is not obvious.

4.4 CONCLUSION

In summary, elastic scattering of protons by ^{64}Zn, ^{66}Zn and ^{68}Zn has been studied. An experiment was performed to find the differential cross sections at different energies to complement existing differential cross sections and polarization data. All these data were analysed with optical model potential. The energy dependence and isospin dependence of the optical model potential were studied by using both the common geometry approach and the volume integral per nucleon. The results of these two approaches indicate that the energy dependences

are almost the same for the three zinc isotopes (-0.332±0.007) and they do not follow the trend of A dependence suggusted by earlier results obtained for ^{40}Ca and ^{208}Pb.

The isospin potential strength obtained from simultaneous search is U_t =-3.8±2.5MeV for data between E = 20MeV and 50MeV. This is much smaller than the value obtained by Perey(pe63) and Becchetti(Be69). The coefficient ζ for the isospin term in the volume integral per nucleon is quite different from the value 0.48 suggested by Greenlees(Gr68). Nuclear structure changes might well affect the determination of the isospin dependence using isotopic sequences. Although there is no drastic change in deformation nor change in shell occupied by the outermost nucleons among the zinc isotopes, it would seem possible that some detail of structure of the zinc nuclei makes it difficult to compare the isospin terms for the zinc isotopes and other nuclei.

APPENDIX

TABLES OF DIFFERENTIAL CROSS SECTIONS

Note:

For the sake of uniformity all cross sections are given to at most 4 significant figures even when the reported errors do not fully justify such precision.

$^{64}Zn(p,p)^{64}Zn$

$E_p = 22.20 \pm 0.15$ MeV

$\theta_{c.m.}$ (deg)	$d\sigma/d\Omega_{c.m.}$ (mb/sr)	error (%)	$\theta_{c.m.}$ (deg)	$d\sigma/d\Omega_{c.m.}$ (mb/sr)	error (%)
10.16	25820.	2.1	90.92	10.70	2.3
12.70	10360.	1.7	93.42	7.592	2.2
15.24	5376.	1.8	95.92	5.271	3.1
17.78	2754.	1.7	98.42	3.207	1.9
20.32	1591.	2.6	100.91	2.059	4.5
22.85	960.1	1.8	103.40	1.737	2.6
25.39	572.3	3.3	105.89	1.994	2.8
27.93	342.0	2.2	108.38	2.526	1.4
30.46	216.6	4.7	110.87	3.167	1.6
33.00	162.6	1.5	113.35	3.829	1.6
35.53	143.9	3.3	115.84	4.352	1.4
38.06	139.7	1.4	118.32	4.616	1.8
40.59	137.0	1.8	120.80	4.606	1.4
43.12	128.6	1.3	123.28	4.366	1.4
45.65	113.7	1.5	125.76	3.972	1.4
48.18	92.62	1.4	128.23	3.388	2.0
50.71	69.55	1.5	130.71	2.744	1.5
53.23	47.50	1.7	133.18	2.116	2.0
55.76	28.25	2.0	135.65	1.592	1.9
58.28	14.38	1.8	138.12	1.155	1.7
60.80	6.536	3.0	140.59	0.976	3.5
63.32	3.695	6.0	143.06	0.875	1.9
65.74	4.822	1.8	145.53	0.942	4.4
68.35	8.328	3.5	148.00	1.079	1.6
70.87	12.68	1.7	150.46	1.305	3.8
73.38	16.89	1.5	152.93	1.570	1.8
75.89	20.02	1.4	155.39	1.836	3.2
78.40	21.70	1.5	157.85	2.065	1.8
80.91	21.23	1.5	160.32	2.138	3.1
83.42	19.62	1.9	162.78	2.225	2.0
85.92	16.83	1.4	165.24	2.288	2.0
88.42	13.36	2.0	167.70	2.289	2.0

$^{64}Zn(p,p)^{64}Zn$

$E_p = 30.00 \pm 0.15$ MeV

$\theta_{c.m.}$ (deg)	$d\sigma/d\Omega_{c.m.}$ (mb/sr)	error (%)	$\theta_{c.m.}$ (deg)	$d\sigma/d\Omega_{c.m.}$ (mb/sr)	error (%)
10.16	14670.	2.0	90.93	2.969	3.0
12.70	6343.	1.8	93.43	2.907	2.2
15.24	3264.	1.7	95.93	3.105	1.7
17.78	1799.	1.6	98.42	3.394	1.5
20.32	903.2	2.2	100.92	3.679	1.4
22.86	380.0	2.8	103.41	3.590	1.4
25.39	128.1	4.7	105.90	3.517	1.4
27.93	48.41	6.2	108.39	3.153	1.4
30.47	55.83	2.5	110.87	2.770	1.6
33.00	97.63	1.4	113.36	2.413	2.1
35.53	137.7	1.4	115.84	1.943	2.5
38.07	175.9	1.7	118.33	1.623	2.8
40.60	160.1	1.4	120.81	1.338	3.4
43.13	139.0	1.4	123.29	1.107	3.8
45.66	105.9	1.5	125.76	0.944	4.1
48.19	71.67	1.6	128.24	0.822	3.8
50.71	43.47	1.8	130.71	0.719	5.7
53.24	22.41	2.1	133.19	0.678	3.1
55.76	11.47	2.0	135.66	0.646	3.3
58.29	8.333	1.5	138.13	0.614	2.3
60.81	10.24	1.8	140.60	0.619	2.2
63.33	14.73	1.7	143.07	0.595	2.1
65.84	19.31	1.5	145.53	0.681	2.1
68.36	21.93	1.4	148.00	0.721	2.1
70.88	22.74	1.5	150.47	0.797	2.6
73.39	21.24	1.5	152.93	0.891	2.6
75.90	17.61	2.2	155.39	0.849	2.7
78.41	14.01	2.1	157.86	0.862	2.6
80.92	9.691	2.5	160.32	0.775	3.2
83.42	6.829	2.9	162.78	0.720	3.5
88,43	3.632	3.3	165.24	0.668	3.7
			167.70	0.595	3.8

$^{64}Zn(p,p)^{64}Zn$

$E_p = 39.60 \pm 0.15$ MeV

$\theta_{c.m.}$ (deg)	$d\sigma/d\Omega_{c.m.}$ (mb/sr)	error (%)	$\theta_{c.m.}$ (deg)	$d\sigma/d\Omega_{c.m.}$ (mb/sr)	error (%)
10.16	8489.	1.9	90.94	2.773	1.7
12.70	4580.	1.6	93.44	2.665	1.8
15.24	2922.	1.7	95.94	2.276	1.9
17.78	1463.	1.8	98.43	1.861	2.3
20.32	552.7	1.8	100.93	1.301	2.4
22.86	154.5	2.9	103.42	0.980	4.4
25.40	24.43	7.0	105.91	0.747	6.0
27.93	35.54	2.1	108.40	0.603	6.8
30.47	107.7	1.8	110.88	0.508	7.1
33.01	165.6	1.7	113.37	0.471	6.6
35.54	186.0	1.6	115.85	0.464	5.2
38.07	174.1	1.5	118.33	0.462	4.2
40.60	128.5	1.5	120.81	0.430	2.7
43.14	86.55	1.7	123.29	0.424	2.9
45.66	51.30	2.2	125.77	0.389	2.7
48.19	26.91	3.0	128.25	0.350	2.6
50.72	14.70	2.4	133.19	0.236	3.3
53.25	11.65	2.1	138.13	0.150	5.2
55.77	13.83	1.6	140.60	0.109	3.2
58.29	17.29	1.6	143.07	0.093	8.7
60.81	18.58	1.5	145.54	0.081	12.
63.33	18.43	1.4	148.00	0.090	11.
65.85	16.15	1.4	150.47	0.111	9.8
68.37	13.12	1.9	152.93	0.130	9.3
70.88	9.711	2.2	155.40	0.155	7.2
73.40	6.497	3.8	157.86	0.173	6.5
75.91	4.503	4.8	160.32	0.170	5.8
78.42	3.286	5.3	162.78	0.181	5.0
80.93	2.632	2.9	165.24	0.177	4.7
83.43	2.511	3.1	167.70	0.176	4.1
85.94	2.658	1.6			
88.44	2.700	1.7			

$^{66}Zn(p,p)^{66}Zn$

$E_p = 22.20 \pm 0.15$ MeV

$\theta_{c.m.}$ (deg)	$d\sigma/d\Omega_{c.m.}$ (mb/sr)	error (%)	$\theta_{c.m.}$ (deg)	$d\sigma/d\Omega_{c.m.}$ (mb/sr)	error (%)
10.16	28920.	3.9	90.90	8.943	2.5
12.69	10330.	2.5	93.39	6.389	2.1
15.23	4957.	1.9	95.89	4.240	3.5
17.77	2746.	1.8	98.39	2.763	2.0
20.31	1649.	2.5	100.88	1.836	10.
22.84	1002.	1.9	103.37	1.695	2.9
25.38	631.6	3.2	105.87	2.024	2.3
27.91	392.1	2.2	108.35	2.607	1.4
30.45	244.2	4.3	110.84	3.233	1.6
32.98	182.4	1.6	113.33	3.924	1.8
35.51	155.2	3.1	115.81	4.395	1.4
38.05	143.5	1.5	118.29	4.624	1.4
40.58	134.7	1.8	120.78	4.544	1.5
43.11	121.2	1.4	123.26	4.337	1.4
45.63	103.7	1.6	125.73	3.871	1.4
48.16	81.79	1.7	128.21	3.258	2.0
50.69	59.06	2.0	130.69	2.639	1.5
53.21	37.58	1.8	133.16	1.971	1.9
55.73	21.83	2.1	135.63	1.413	2.5
58.26	10.71	1.7	138.11	0.958	1.7
60.78	4.709	2.8	140.58	0.667	5.8
63.29	3.637	7.4	143.05	0.619	1.9
65.81	5.800	1.9	145.51	0.623	6.9
68.33	9.565	3.1	147.98	0.843	1.7
70.84	14.66	1.5	150.45	1.101	4.2
73.35	18.57	1.4	152.91	1.440	1.8
75.87	20.79	1.4	155.38	1.719	2.9
78.37	21.35	1.6	157.84	1.999	1.8
80.88	20.43	1.6	160.31	2.109	2.6
83.39	17.99	2.0	162.77	2.255	2.0
85.89	14.86	1.8	165.23	2.264	2.0
88.39	11.79	2.1	167.69	2.212	2.0

$^{66}Zn(p,p)^{66}Zn$

$E_p = 30.00 \pm 0.15$ MeV

$\theta_{c.m.}$ (deg)	$d\sigma/d\Omega_{c.m.}$ (mb/sr)	error (%)	$\theta_{c.m.}$ (deg)	$d\sigma/d\Omega_{c.m.}$ (mb/sr)	error (%)
10.16	13800.	2.3	90.90	2.752	2.7
12.70	6103.	1.7	93.40	3.057	2.0
15.23	3145.	1.7	95.90	3.411	1.6
17.77	1730.	1.7	98.40	3.736	1.6
20.31	837.8	2.2			
22.85	343.5	2.9	103.38	3.818	1.4
25.38	128.1	4.7	105.87	3.373	1.5
27.92	58.18	5.8	108.36	2.916	1.7
30.45	71.05	2.4	110.85	2.420	1.8
32.99	112.7	1.5	113.33	1.931	2.3
35.52	149.0	1.5	115.82	1.570	2.8
38.05	164.0	1.5	118.30	1.230	5.4
40.58	157.2	1.4	120.78	1.050	4.0
43.11	129.5	1.5	123.26	0.937	4.3
45.64	95.20	1.6	125.74	0.863	4.2
48.17	61.03	1.8	128.22	0.791	5.7
50.69	34.34	1.9			
53.22	16.27	2.2	133.17	0.775	2.9
55.74	8.554	1.8	135.64	0.684	2.6
58.26	8.110	1.9	138.11	0.627	2.5
60.78	12.10	1.8	140.58	0.578	2.1
63.30	17.19	1.7	143.05	0.557	2.3
65.82	21.25	1.5	145.52	0.548	2.3
68.33	23.11	1.5	147.98	0.593	2.5
70.85	22.38	1.5	150.45	0.691	2.2
73.36	19.52	2.3	152.92	0.788	2.4
75.87	16.30	2.3	155.38	0.800	2.6
78.38	12.21	1.9	157.85	0.825	5.0
80.88	8.600	2.5	160.31	0.797	2.8
83.40	5.515	3.2	162.77	0.782	3.1
85.90	3.816	3.4	165.23	0.746	3.2
88.40	2.822	3.6	167.70	0.684	5.4

$^{66}Zn(p,p)^{66}Zn$

$E_p = 39.60 \pm 0.15$ MeV

$\theta_{c.m.}$ (deg)	$d\sigma/d\Omega_{c.m.}$ (mb/sr)	error (%)	$\theta_{c.m.}$ (deg)	$d\sigma/d\Omega_{c.m.}$ (mb/sr)	error (%)
10.16	10400.	1.8	90.91	2.656	1.7
12.70	5353.	1.7	93.41	2.434	1.5
15.24	2858.	1.7	95.91	2.014	1.8
17.77	1374.	1.8	98.40	1.543	1.8
20.31	527.7	2.0	100.90	1.147	1.5
22.85	133.8	2.1	103.39	0.873	5.5
25.39	20.56	8.4	105.88	0.702	6.2
27.92	48.25	1.8	108.37	0.598	6.3
30.46	110.8	1.9	110.86	0.534	5.8
32.99	167.6	1.6	113.34	0.522	4.6
35.52	182.5	1.6	115.83	0.513	3.7
38.06	163.8	1.6	118.31	0.507	2.8
40.59	120.8	1.7	120.79	0.479	2.1
43.12	78.09	1.9	123.27	0.426	2.5
45.64	42.90	2.5	125.75	0.384	2.8
48.17	20.62	1.6	128.22	0.375	2.4
50.70	12.62	3.1			
53.22	12.00	1.7	133.17	0.228	4.4
55.75	15.49	1.7	135.64	0.195	4.4
58.27	18.94	1.8	138.12	0.152	5.4
60.79	19.58	1.5	140.59	0.130	5.8
63.31	18.50	1.5	143.05	0.108	4.4
65.83	15.91	1.6	145.52	0.106	7.0
68.34	11.75	2.2	147.99	0.109	7.3
70.86	8.608	2.9	150.46	0.118	7.9
73.37	5.514	1.9	152.92	0.146	7.2
75.88	3.754	5.5	155.39	0.160	6.7
78.39	2.867	5.3	157.85	0.180	6.0
80.90	2.652	3.9	160.31	0.186	5.5
83.40	2.703	2.3	162.77	0.196	5.0
86.91	2.802	1.7	165.24	0.190	3.7
88.41	2.720	1.6	167.70	0.182	4.7

$^{68}Zn(p,p)^{68}Zn$

$E_p = 22.20 \pm 0.15$ MeV

$\theta_{c.m.}$ (deg)	$d\sigma/d\Omega_{c.m.}$ (mb/sr)	error (%)	$\theta_{c.m.}$ (deg)	$d\sigma/d\Omega_{c.m.}$ (mb/sr)	error (%)
10.15	34010.	2.3	90.87	8.419	2.6
12.69	11950.	2.1	93.37	5.338	2.0
15.23	5699.	1.9	95.67	3.450	3.4
17.76	3191.	1.9	98.36	2.354	2.6
20.30	1907.	2.4	100.86	1.840	8.4
22.83	1190.	2.0	103.35	2.059	2.4
25.37	746.1	2.9	105.84	2.629	1.7
27.90	469.0	2.3	108.33	3.305	1.5
30.43	294.2	3.8	110.82	3.961	1.6
32.97	219.4	1.7	113.30	4.567	1.5
35.50	184.6	2.6	115.79	4.879	1.5
38.03	167.0	1.5	118.27	5.028	1.5
40.56	149.2	1.7	120.75	4.785	1.5
43.09	132.3	1.5	123.23	4.387	2.1
45.61	110.0	1.6	125.71	3.854	1.6
48.14	79.94	1.6	128.19	3.165	2.0
50.67	57.85	1.7	130.67	2.433	2.0
53.19	35.66	2.0	133.14	1.746	1.9
55.71	19.17	2.2	135.61	1.145	3.6
58.23	8.423	2.0	138.09	0.743	1.7
60.75	4.261	2.1	140.56	0.496	8.7
63.27	4.851	7.1	143.03	0.410	2.0
65.79	8.668	2.1	145.50	0.529	15.
68.30	13.83	2.4	147.97	0.772	1.7
70.82	19.11	1.6	150.43	1.122	3.9
73.33	22.70	1.5	152.90	1.513	2.0
75.84	24.59	1.6	155.37	1.854	2.3
78.35	23.87	1.8	157.83	2.144	2.0
80.86	21.82	1.7	160.30	2.265	2.0
83.36	18.52	2.1	162.76	2.399	2.0
85.87	14.94	2.0	165.22	2.387	2.0
88.37	11.17	2.2	167.69	2.288	2.0

$^{68}Zn(p,p)^{68}Zn$

$E_p = 30.00 \pm 0.15$ MeV

$\theta_{c.m.}$ (deg)	$d\sigma/d\Omega_{c.m.}$ (mb/sr)	error (%)	$\theta_{c.m.}$ (deg)	$d\sigma/d\Omega_{c.m.}$ (mb/sr)	error (%)
10.15	12730.	2.6	90.88	3.231	2.3
12.69	6087.	2.1	93.38	3.762	1.8
15.23	3902.	1.9	95.87	4.214	1.7
17.76	1986.	2.1	98.37	4.507	1.6
20.30	975.3	2.3			
22.84	423.8	3.0	103.36	4.044	1.7
25.37	155.8	4.7	105.85	3.535	1.7
27.90	79.85	5.0			
30.44	92.25	2.3	110.82	2.195	2.2
32.97	143.6	1.8	113.31	1.657	2.8
35.50	181.3	1.7	115.79	1.251	3.7
38.03	192.2	1.8	118.28	1.001	4.6
40.56	180.4	1.8	120.76	0.903	4.9
43.09	138.5	1.8	123.24	0.885	4.6
45.62	99.31	1.9	125.72	0.906	4.2
48.15	59.87	2.3	128.20	0.944	3.3
50.67	30.15	2.6			
53.20	13.20	2.3	133.15	0.891	2.7
55.72	8.261	1.7	135.62	0.817	2.3
58.24	10.58	2.1	138.09	0.702	2.4
60.76	16.59	2.5	140.56	0.517	3.4
63.28	22.09	2.0			
65.79	26.15	1.8			
68.31	26.71	1.8			
70.82	25.30	1.8	150.44	0.546	2.7
73.34	21.38	1.8	152.90	0.615	2.9
75.85	16.63	1.9	155.37	0.719	3.7
78.36	11.59	2.3	157.84	0.775	3.0
80.86	7.757	2.9	160.30	0.880	2.9
83.37	4.707	4.0	162.76	0.890	3.0
85.87	3.393	4.0	165.23	0.912	3.6
88.38	2.904	3.2	167.69	0.853	2.9

$^{68}Zn(p,p)^{68}Zn$

$E_p = 39.6 \pm 0.15$ MeV

$\theta_{c.m.}$ (deg)	$d\sigma/d\Omega_{c.m.}$ (mb/sr)	error (%)	$\theta_{c.m.}$ (deg)	$d\sigma/d\Omega_{c.m.}$ (mb/sr)	error (%)
10.15	10130.	1.6	90.88	3.017	1.6
12.69	5156.	1.6	93.38	2.496	1.8
15.23	2721.	1.7	95.88	1.984	2.5
17.77	1207.	1.9	98.38	1.483	3.6
20.30	444.8	2.1	100.87	1.164	2.2
22.84	89.70	6.2	103.36	0.879	6.0
25.37	20.11	11.	105.85	0.729	6.0
27.91	77.64	1.8	108.34	0.693	2.0
30.44	157.6	1.8	110.83	0.637	4.3
32.98	211.7	1.7	113.32	0.638	3.1
35.51	215.8	1.6	115.80	0.620	2.6
38.04	179.9	1.6	118.28	0.578	2.2
40.57	130.9	1.9	120.77	0.523	2.0
43.10	77.87	2.1	123.25	0.460	2.5
45.63	39.84	2.9	125.72	0.414	3.0
48.15	19.09	3.8	128.20	0.408	3.0
50.68	13.25	1.9	130.68	0.282	2.1
53.20	15.70	1.6	133.15	0.248	4.4
55.72	20.35	2.0			
58.25	24.44	1.8	138.10	0.181	4.9
60.77	24.52	1.5	140.57	0.169	2.9
63.28	22.19	1.5	143.04	0.152	2.0
65.80	17.71	2.0			
68.32	12.57	2.5	147.98	0.139	2.0
70.83	8.252	2.7	150.44	0.151	4.5
73.34	5.331	5.0	152.91	0.158	4.9
75.85	3.742	5.7			
78.36	3.236	4.4	157.84	0.200	4.9
80.87	3.212	2.3	160.32	0.212	5.2
83.38	3.525	1.8	162.77	0.223	5.0
85.88	3.580	1.8			
88.38	3.471	1.8	167.69	0.203	5.3

REFERENCES

Be64 J. Benveniste, A. C. Mitchell, B. Buck, and C. B. Fulmer, Phys. Rev. B133(1964)323.

Be69 F. D. Becchetti Jr. and G. W. Greenlees, Phys. Rev. 182(1969)1190.

@@1

Bo72 R. N. Boyd, J. C. Lombardi, R. Mohan, R. Arking and A. B. Robbins, Nucl. Phys. A181(1972)571.

Bu65 J. J. Burgerjon, F. Konopasek and K. G. Standing. IEEE Trans. Nucl. Sci. 12(1965)334.

Ca67 M. Calderbank et al., Nucl Phys. A105(1967)601

Du65 J. E. Durisch and P. Gould. Phys. Rev. B137(1965)906.

Fe54 H. Feshbach, C. E. Porter and V. F. Weisskoff, Phys. Rev. 96(1954)488.

Fe58 H. Feshbach, Ann. Rev. of Nucl. Sci. 8(1958)49.

Fr67 M. P. Fricke et al., Phys. Rev. 156(1967)1207.

Fu69 C. B. Fulmer, J. B. Ball, A. Scott and H. C. Whiten, Phys. Rev. 181(1969)1565.

Fu70 C. B. Fulmer, F. G. Kingston, A. Scott and J. C. Hafele, Phys. Lett. B32(1970)454.

Gr68 G. W. Greenlees, G. J. Pyle and Y. C. Tang, Phys. Rev. 171(1968)1115.

He70 E. Hentschel and G. Heinrich, Nucl. Phys. A144(1970)92.

Ho66 P. E. Hodgson, Adv. Phys. 15(1966)329.

Ho67 P. E. Hodgson, Ann. Rev. of Nucl. Sci. 17(1967)1.

Ho70 P. E. Hodgson, Nucl. Phys. A150(1970)1.

Hu72 H. Huang, M. Sc. thesis, University of Manitoba, 1972, unpublished.

Ke59 A. K. Kerman, H. McManus, and R. M. Thaler, Ann. Phys. 8(1959)551

Ke64 J. G. Kelly, et al.,
Bull. Am. Phys. Soc. 9(1964)544.

La62 A. M. Lane, Phys. Rev. Lett. 8(1962)171.

Le67 V. E. Lewis, E. J. Burge, A. A. Rush, and
D. A. Smith, Nucl. Phys. A101(1967)589.

Li70 H. S. Liers, R. N. Boyd, C. H. Poppe, J. A. Sievers,
and D. L. Watson, Phys. Rev. C2(1970)1399.

Lo70 G. LoBianco, M. Sc. Thesis, University of
Manitoba, 1970.(unpublished)

Ma68 W. Makofske, W. Savin, H. Ogata, and
T. H. Kruse, Phys. Rev. 174(1968)1429.

Ma71 G. S. Mani et al., Nucl. Phys. A165(1971)384.

Ma72 W. Makofske, G. W. Greenlees, F. S. Liers,
and G. J. Pyle, Phys. Rev. C5(1972)780.

Me66 M. S. Melkanoff, J. Raynal, and T. Sawada,
UCLA Report No.66-10(unpulished).

Pe62 F. G. Perey and B. Buck,
Nucl. Phys. 32(1962)353.

Pe63 F. G. Perey, Phys. Rev. 131(1963)745.

Pe68 C. M. Perey, F. G. Perey, J. K. Dickens, and
R. J. Silva, Phys. Rev. 175(1968)1460.

Ro63 L. Rosen and L. Stwart,
Phys. Rev. Lett. 10(1963)246.

Sc66 H. Schulz and H. Wiebricke,
Phys. Lett. 21(1966)190.

Si70 B. C. Sinha and V. R. W. Edwards,
Phys. Lett. 31B(1970)273.

Si72 B. C. Sinha, V. R. W. Edwards, and E. J. Burge,
Nucl. Phys. A183(1972)401.

Sm64 R. Smyth, Rev. Sci. Instr. 35(1964)1197.

So65 P. C. Sood, Phys. Lett. 19(1965)52.

Ta63 Y. C. Tang, E. Schmid, and K. Wildermuth,
Phys. Rev. 131(1963)2631

Va69 W. T. H. van Oers and J. M. Cameron,
Phys. Rev. 184(1969)1061.

Va71 W. T. H. van Oers, Phys. Rev. C3(1971)1551.

Wi66 H. Willmes, Nucl. Instr. 41(1966)122

Wo54 R. D. Woods and D. S. Saxon,
Phys. Rev. 95(1954)577.

Zi68 J. Zimanji and B. Gyrmali,
Phys. Rev. 174(1968)1112.

Br71 K. H. Bray et al., Nucl. Phys. A167(1971)57.

Va74 W. T. H. van Oers et al., Phys. Rev. c10(1974)307.